June 4, 2018
Preprint typeset using LaTeX style emulateapj v. 11/10/09

PUSHING THE BOUNDARIES OF CONVENTIONAL CORE-COLLAPSE SUPERNOVAE: THE EXTREMELY ENERGETIC SUPERNOVA SN 2003ma

A. Rest[1,2], R. J. Foley[3,4], S. Gezari[5,6], G. Narayan[1], B. Draine[7], K. Olsen[8,9], M. E. Huber[5,10], T. Matheson[9], A. Garg[10,11], D. L. Welch[12], A. C. Becker[13], P. Challis[3,10], A. Clocchiatti[14], K. H. Cook[10,11], G. Damke[10,15], M. Meixner[10,16], G. Miknaitis[10,17], D. Minniti[14], L. Morelli[18], S. Nikolaev[11], G. Pignata[19], J. L. Prieto[10,20,21,22], R. C. Smith[8], C. Stubbs[1], N. B. Suntzeff[23], A. R. Walker[8], W. M. Wood-Vasey[10,24], A. Zenteno[10,25,26], L. Wyrzykowski[27], A. Udalski[28], M. K. Szymański[28], M. Kubiak[28], G. Pietrzyński[28,29], I. Soszyński[28], O. Szewczyk[28,29], K. Ulaczyk[28], R. Poleski[28]

June 4, 2018

ABSTRACT

We report the discovery of a supernova (SN) with the highest apparent energy output to date and conclude that it represents an extreme example of the Type IIn subclass. The SN, which was discovered behind the Large Magellanic Cloud at $z = 0.289$ by the SuperMACHO microlensing survey, peaked at $M_R = -21.5$ mag and only declined by 2.9 mag over 4.7 years after the peak. Over this period, SN 2003ma had an integrated bolometric luminosity of 4×10^{51} ergs, more than any other SN to date. The radiated energy is close to the limit allowed by conventional core-collapse explosions. Optical spectra reveal that SN 2003ma has persistent single-peaked intermediate-width hydrogen lines, a signature of interaction between the SN and a dense circumstellar medium. The light curves show further evidence for circumstellar interaction, including a long plateau with a shape very similar to the classic SN IIn 1988Z – however, SN 2003ma is ten times more luminous at all epochs. The fast velocity measured for the intermediate-width Hα component ($\sim$6000 km s^{-1}) points towards an extremely energetic explosion ($> 10^{52}$ ergs), which imparts a faster blast-wave speed to the post-shock material and a higher luminosity from the interaction than is observed in typical SNe IIn. Mid-infrared observations of SN 2003ma suggest an infrared light echo is produced by normal interstellar dust at a distance $\sim$0.5 pc from the SN.

Subject headings: circumstellar matter — supernovae: individual (SN 2003ma) — dust, extinction

[1] Department of Physics, Harvard University, 17 Oxford Street, Cambridge, MA 02138, email: arest@physics.harvard.edu
[2] Space Telescope Science Institute, 3700 San Martin Dr., Baltimore, MD 21218
[3] Harvard-Smithsonian Center for Astrophysics, 60 Garden St., Cambridge, MA 02138
[4] Clay Fellow
[5] Department of Physics and Astronomy, Johns Hopkins University, 3400 N. Charles St., Baltimore, MD 21218
[6] Hubble Fellow
[7] Dept. of Astrophysical Sciences, Princeton University, Princeton, NJ 08544
[8] Cerro Tololo Inter-American Observatory, National Optical Astronomy Observatory (CTIO/NOAO), Colina el Pino S/N, La Serena, Chile
[9] National Optical Astronomy Observatory, 950 N. Cherry Ave., Tucson, AZ 85719-4933
[10] Visiting Astronomer, Cerro Tololo Inter-American Observatory, National Optical Astronomy Observatory, which is operated by the Association of Universities for Research in Astronomy, Inc. (AURA) under cooperative agreement with the National Science Foundation
[11] Lawrence Livermore National Laboratory, 7000 East Ave., Livermore, CA 94550
[12] Dept. of Physics and Astronomy, McMaster University, Hamilton, Ontario, L8S 4M1, Canada
[13] Dept. of Astronomy, University of Washington, Box 351580, Seattle, WA 98195
[14] Dept. of Astronomy, Pontificia Universidad Católica de Chile, Casilla 306, Santiago 22, Chile
[15] Department of Astronomy, University of Virginia, P.O. Box 400325, Charlottesville, VA 22904-4325
[16] STScI, 3700 San Martin Dr., Baltimore, MD 21218
[17] Center for Neighborhood Technology, 2125 W. North Ave., Chicago IL 60647
[18] Dipartimento di Astronomia, Università di Padova, vicolo dell'Osservatorio 3, I-35122 Padova, Italy
[19] Departamento de Ciencias Fisicas, Universidad Andres Bello, Avda. Republica 252, Santiago, Chile
[20] Dept. of Astronomy, Ohio State University, 140 West 18th Ave., Columbus, OH 43210-1173
[21] Carnegie Observatories, 813 Santa Barbara St., Pasadena, CA 91101
[22] Hubble and Carnegie-Princeton fellow
[23] Dept. of Physics, Texas A&M University, College Station, TX 77843-4242
[24] Dept. of Physics and Astronomy, University of Pittsburgh, 3951 O'Hara St., Pittsburg, PA 15260
[25] Department of Physics, Ludwig-Maximilians-Universität, Scheinerstr. 1, 81679 München, Germany
[26] Excellence Cluster Universe, Boltzmannstr. 2, 85748 Garching, Germany
[27] Institute of Astronomy, University of Cambridge, Madingley Road, Cambridge CB3 0HA, UK
[28] Warsaw University Astronomical Observatory, Al. Ujazdowskie 4, 00-478 Warszawa, Poland
[29] Universidad de Concepción, Departamento de Fisica,Astronomy Group, Casilla 160-C, Concepción, Chile

1. INTRODUCTION

Hydrogen-rich (Type II) core-collapse supernovae (SNe) from massive stars typically have peak luminosities corresponding to absolute magnitudes $-14 > M_R > -18$ mag that are powered by thermal energy that is deposited into the expanding SN envelope during shock breakout (Li et al. 2010). Depending on the mass of the hydrogen (H) envelope, a plateau can arise in the optical light curve from a cooling wave of H recombination that recedes through the ejecta layers. After this photospheric phase, the light curve displays an exponential decline when it is predominantly powered by the radioactive decay of isotopes created in the explosion (^{56}Ni $\rightarrow^{56}$Co $\rightarrow^{56}$Fe).

In the presence of a dense circumstellar medium (CSM), the expanding SN shock will collide with the CSM and convert the bulk kinetic energy of the explosion into light (Chevalier & Fransson 1994), and produce a relatively narrow (2 – 4 $\times 10^3$ km s^{-1}) Hα line that is the hallmark of SNe IIn (Schlegel 1990). The additional luminosity from the circumstellar interaction can be extremely large and even dominate the total luminosity. Furthermore, while the luminosity from radioactive decay will decline quickly after a few months, the luminosity from circumstellar interaction can persist at a near-constant level for several years.

Recently, several extremely luminous SNe have emerged with peak luminosities with $M_R < -21$ mag. SN 2006gy had a very long rise time (70 days) and peaked at $M_R = -21.8$ mag (Smith et al. 2007b; Ofek et al. 2007). SN 2008fz had a similar peak brightness ($M_{\rm V} = -22.3$ mag) and light-curve shape (Drake et al. 2010). SN 2005ap was very luminous at peak ($M_{\rm unf} = -22.7$ mag), but had a fast rise and decay. SN 2008es was similar to SN 2005ap, peaking at $M_V = -22.3$ mag and having a fast rise and decline (Miller et al. 2009; Gezari et al. 2009a). A self-obscured luminous supernova, SN 2007va, was detected by Kozłowski et al. (2010) only in the infrared with an absolute mid-IR peak magnitude of $M_{[4.5]} \approx -24.2$. More recently, Quimby et al. (2009) and Gal-Yam et al. (2009) announced the discovery of three extremely luminous SNe, respectively, which they suggest are powered by a pulsational pair instability (Woosley et al. 2007). Pastorello et al. (2010) finds evidence that these extremely luminous SNe may be connected to SN Ic.

A pulsational pair instability is expected to be important in only the most massive stars – those exceeding 95 $M_\odot$. The production of electron-positron pairs results in a contraction and then explosive nuclear burning which ejects some significant number of solar masses worth of material from the envelope. Subsequent repetitions of this sequence of events result in ejected shells catching up with previous ejected material, now at much larger radius, producing radiated energy due to the shell collisions. This process is estimated to be capable of producing 10^{50} ergs of light and, as importantly, can repeat on short timescales, providing longer-timescale luminosity.

The energetics of these events push the envelope of our understanding of stellar evolution. The peak luminosity, if powered by radioactive decay, would require $\sim$10 $M_\odot$ of ^{56}Ni. This very large amount points to an extremely massive progenitor and the possibility that these events were the result of a pair-instability SN (Barkat et al. 1967; Bond et al. 1984). Alternatively, a significant amount of the luminosity may be produced by circumstellar interaction, but the mass of the CSM necessary for the luminosity still indicates that the progenitors must have been massive stars with significant mass-loss histories.

Furthermore, there is a limit on the energy for which conventional core-collapse explosions are viable. Under a conventional core-collapse explosion, the maximum energy emitted by a SN is equivalent to the rest mass of a neutron star, a few 10^{54} ergs, with 99% being emitted as neutrinos (e.g., Woosley & Janka 2005). The remaining energy, a few 10^{52} ergs, is either coupled to the baryonic material as kinetic energy, or emitted as electromagnetic radiation. If a SN has demonstrably greater than a few 10^{52} ergs, the conventional core-collapse scenario must be re-examined. This argument has been used for the extremely energetic broad-lined SNe Ic associated with gamma-ray bursts (e.g., Woosley 1993; Iwamoto et al. 1998); although these constraints are placed on this class of objects using the kinetic energy, not the radiated energy.

In the local universe, there have been several well-observed SNe IIn: SNe 1988Z (Turatto et al. 1993), 1994W (Sollerman et al. 1998), 1995N (Fransson et al. 2002), 1998S (e.g., Leonard et al. 2000), 1999el (Di Carlo et al. 2002), 2005ip (Smith et al. 2009b), and 2007rt (Trundle et al. 2009). In addition to their similar spectral evolution, SNe IIn all have long plateaus in their light curves after an initial decline. This plateau is from shock energy being continuously converted into visual light through circumstellar interaction. Once the shock extends to a radius where the density of the CSM drops, the source of the luminosity is diminished and the SN fades significantly.

Observations suggest that dust can form in the ejecta of SNe (Moseley et al. 1989; Kozasa et al. 1989; Sugerman et al. 2006; Smith et al. 2008b; Rho et al. 2008; Fox et al. 2009; Kotak et al. 2009). This process appears to be enhanced by increasing the density of the CSM; i.e., SNe IIn appear to be better at forming dust than SNe IIP. An infrared light echo can appear at late times when light from the SN explosion reaches a dust shell, and the UV/optical light is reprocessed into the infrared (e.g., Gerardy et al. 2002a).

Here we present SN 2003ma, discovered behind the LMC by the SuperMACHO microlensing survey. SN 2003ma has the light curve shape and spectral signatures of a SN IIn, but with a peak luminosity comparable to the most luminous SNe ever discovered. In Section 2 we describe the densely-sampled SuperMACHO and OGLE-III difference imaging photometry (covering a baseline of 12 years, and the SN light curve over 4.7 years), and spectroscopy taken at the peak of the SN, and 1, 2, 5, and 6 years later, and in Section 3 we compare the observations to well studied SNe IIn. In Section 4 we calculate the total bolometric luminosity and energy output of the SN, and show that it exceeds the radiative output of any other SN observed to date. We compare possible models for the source of the energy, and show evidence for an IR echo from variable IR flux measured

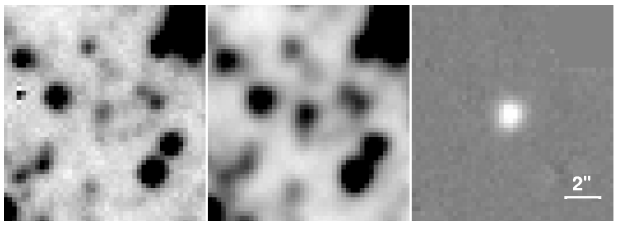

FIG. 1.— SuperMACHO images of the region around SN 2003ma. Left: Template image from 2001 November 20 (pre-event). Middle: Search image from 2003 December 17, showing a detection of SN 2003ma at the center of the image. Right: Difference image (center minus left with an inverted color scale) clearly showing the detection of SN 2003ma. The white line in the lower right corner indicates 2″. North is up and East is left.

in archival *Spitzer* IRAC observations. In Section 5, we summarize our results.

2. OBSERVATIONS & REDUCTIONS

2.1. *Optical Photometry*

Starting in 2001, the SuperMACHO Project microlensing survey used the CTIO 4 m Blanco telescope with its 8K × 8K MOSAIC imager (plus its atmospheric dispersion corrector) to monitor the central portion of the LMC every other night for 5 seasons (September through December). The images were taken through our custom "*VR*" filter (λ_c = 625 nm, $\delta\lambda$ = 220 nm; NOAO Code c6027) with exposure times between 60 and 200 seconds, depending on the stellar density of each field. In addition to the *VR* filter, images were occasionally obtained through the *B* and *I* filters. Throughout this paper, we denote brightnesses measured in the natural CTIO magnitude system as $B_{\rm SM}$, $VR_{\rm SM}$ and $I_{\rm SM}$ as defined in Miknaitis et al. (2007). To search for variability, PSF-matched template images were subtracted from search images (Rest et al. 2005; Garg et al. 2007; Miknaitis et al. 2007). The resulting difference images are remarkably clean of the (constant) stellar background and are ideal for searching for variable objects. Our pipeline detects and catalogs all variable sources.

On 2003 December 13, the SuperMACHO survey detected a non-microlensing transient event at position RA = 05:31:01.878, Dec = −70:04:15.89 with a *VR* magnitude of 20.53. The panels in Figure 1 show from left to right cut-outs from a pre-event image (2001 November 20), an image 4 days after discovery (∼6 days before the peak; 2003 December 17), and their difference image, respectively. The event position in the difference images is 0.064 ± 0.012 arcsec to the south of a source (the presumed host galaxy) in the pre-event template image (see Figure 2). At a redshift of $z = 0.289$ of SN 2003ma and its host (see Section 2.3), this corresponds to a projected distance of $d \approx 460 \pm 85$ pc. The host galaxy has apparent magnitudes of $B_{SM} = 20.93 \pm 0.06$ mag, $VR_{SM} = 20.15 \pm 0.02$ mag, and $I_{SM} = 19.76 \pm 0.03$ mag.

SN 2003ma was also detected by the OGLE–III survey (2001 – 2009), which is a photometric survey using a dedicated 1.3-m Warsaw telescope located at the Las Campanas Observatory, Chile, operated by the Carnegie Institution of Washington. The camera uses eight SITe 2048×4096 CCD detectors with 15 μm pixels resulting in 0.26 arcsec pixel^{-1} scale and 35×35 arcmins total field of view. For the details of the instrumentation setup

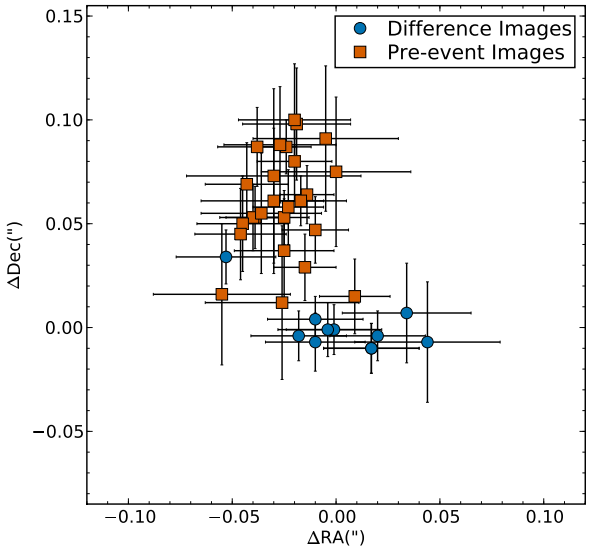

FIG. 2.— Centroids of the sources at/near the position of SN 2003ma from multiple images. The red squares indicate the centroids of detections in the pre-event (MJD ≤ 52965) SuperMACHO images, while the blue circles indicate the high S/N centroids of SN 2003ma in the SuperMACHO difference images during 52985 ≤ MJD ≤ 53020. SN 2003ma is offset from the template source by 0.064 ± 0.012 arcsec, indicating that it is at a projected distance of $d \approx 460 \pm 85$ pc from the host.

we refer the reader to Udalski (2003). Approximately 500 photometric points per star towards the LMC were accumulated over eight seasons, between July 2001 and May 2009. Most of the observations were carried through the Cousins *I*-band filter with exposure times 180 seconds. Full description of the reduction techniques, difference image analysis, photometric calibration and astrometric transformations can be found in Wozniak (2000); Udalski et al. (2008).

Pre-event *I*-band data were also gathered during the OGLE–II survey (1996 – 2000), which used the same dedicated telescope as OGLE–III, but was equipped with a single 2048×2048 CCD (Udalski et al. 1997). Since the QE of the two CCD's are slightly different, we apply a small 2% correction to the OGLE–II data so that their average flux matches the pre-event flux in the OGLE–III. Since the OGLE-II data is several years before the event, we used it to test for pre-event variability, for example caused by an active galactic nucleus (AGN).

The upper and lower panels of Figure 3 shows the difference image light curves from the SuperMACHO and OGLE surveys. Images with poor seeing and/or significant cloud cover are more likely to have large (and non-Poissonian) systematic uncertainties. Therefore, only images with seeing better than 1.5″ and with atmospheric extinction less than 1 mag are used for the analysis. We make an exception for images from July and August 2008, which typically have poor seeing, but are crucial for understanding the late-time behavior of SN 2003ma. For these months, images with seeing better than 1.9″ were retained. Since there are several images in all filters from 2008, we were able to average the flux from these images.

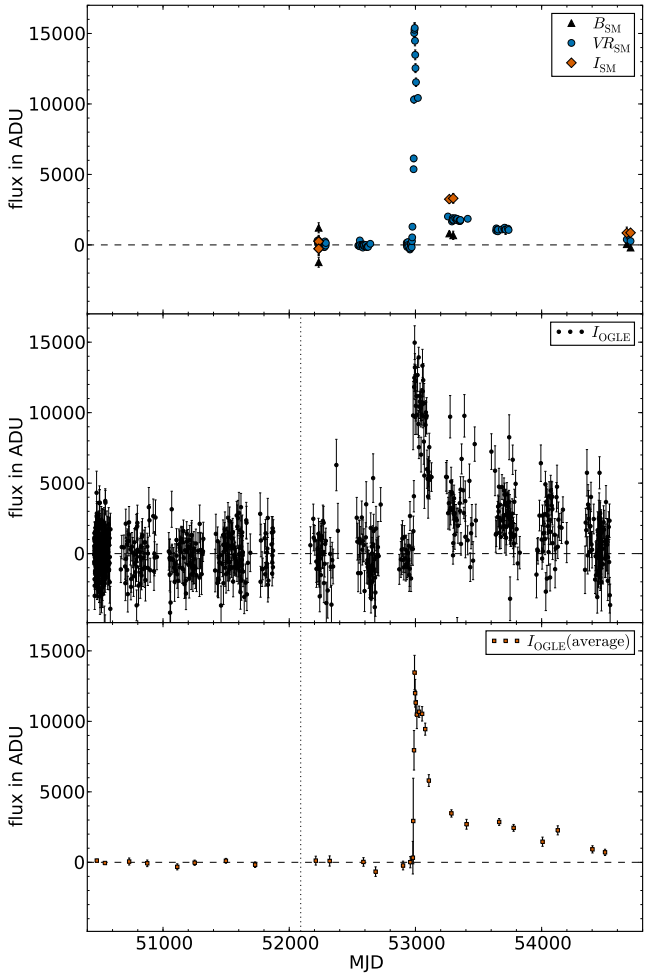

FIG. 3.— Difference image light curves of SN 2003ma. Top: Black triangles, blue circles, and orange diamonds show the SuperMACHO difference flux light curves in B_{SM}, VR_{SM}, and I_{SM}, respectively, from 2001 November 11 to 2008 August 25. Middle: Small black circles indicate the I_{OGLE} difference flux light curves. Bottom: Because of the low S/N of a single detection, we average the data (orange squares). The horizontal dashed lines indicate zero flux. The vertical dotted line indicates the transition between OGLE–II and OGLE–III measurements.

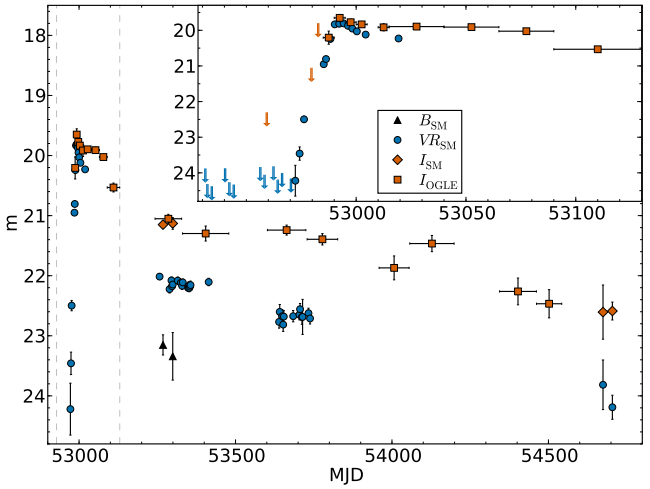

FIG. 4.— Optical light curves of SN 2003ma. The black triangles, blue circles, orange diamonds, and orange squares show the apparent magnitudes in the natural system of B_{SM}, VR_{SM}, I_{SM}, and I_{OGLE}, respectively. Because of the low S/N of a single detection, we average I_{OGLE} (orange squares), with the range of epochs used to calculate this average indicated by the error bars along the time axis. The inset shows the light curve during peak from $52928 \leq \text{MJD} \leq 53130$, and the 3σ brightness upper limits.

Because difference imaging reveals more instrumental and reduction artifacts than there are real variable objects in an image, standard profile-fitting software package, like DoPHOT (Schechter et al. 1993), have problems determining the optimal PSF in the difference image. To remedy this, we implement a customized version of DoPHOT that uses the applicable PSF from the original image (Rest et al. 2005; Garg et al. 2007). After an object is detected in any difference image we "force" photometry in all difference images at the event position regardless of the flux level. We thus measure the flux in pre-event images and negative fluxes are possible. These measurements are critical for constraining the light curves. For example the pre-event light curve (MJD < 52970) is consistent with no variability, indicating that the host galaxy has not demonstrated a history of variability that would indicate the presence of an AGN.

In addition to the SuperMACHO *VR* images, several *B* and *I* images were obtained on 2001 November 20, 2004 September 20, 2004 October 21, 2008 July 27, and 2008 August 26. The images from 2001 November 20, obtained before the event, are used as the template images for these filters.

The middle panel of Figure 3 shows the OGLE *I*-band difference image photometry (small black circles). Mainly because of the difference in telescope aperture (1.3 m for OGLE and 4 m for SuperMACHO), the signal-to-noise ratio (S/N) of the OGLE photometry is significantly lower than that of the SuperMACHO data. To obtain measurements with sufficient S/Ns, we have binned the OGLE data (lower panel of Figure 3). Since the OGLE observations are taken in blocks, we divide each block in two equal parts, each containing the same amount of measurements. The only exception is during peak, where the S/N of the measurements is significantly higher, and in addition the light curve evolves faster. Thus around peak (52975 <= MJD <= 53015), we average the data in 5-day bins, and in 25-day bins in the range 53015 < MJD <= 53150. In the following analysis, we only use the averaged OGLE data.

We convert the CTIO 4 m difference flux detections into apparent magnitudes (see Figure 4 and Table 1) in the natural CTIO 4 m magnitude system, and we correct for extinction as described in Section 4.1. The OGLE measurements have been converted into standard I-band magnitudes using the standard OGLE photometric calibration (Wozniak 2000; Udalski et al. 2008).

2.2. *Infrared Photometry*

We use archived images and catalogs from the *Spitzer* Space Telescope *SAGE* survey of the LMC (Meixner et al. 2006) to measure the mid-infrared photometry of SN 2003ma. The *SAGE* survey covered a $7^\circ \times 7^\circ$ region centered on the LMC during two epochs, 2005 July 15 – 26 (epoch 1) and 2005 October 26 – November 2 (epoch 2) for its IRAC observations, and 2005 July 27 – August 3 (epoch 1) and 2005 November

TABLE 1
Apparent magnitudes of SN 2003ma

MJD	$B_{\rm SM}$	$VR_{\rm SM}$	$I_{\rm SM}$	$I_{\rm OGLE}$
52959.29126	···	···	···	< 22.30
52964.27804	···	< 24.19	···	···
52966.28245	···	< 24.01	···	···
52970.30195	···	< 24.16	···	···
52972.29799	···	24.22 (0.43)	···	···
52974.25935	···	23.46 (0.19)	···	···
52976.26257	···	22.50 (0.09)	···	···
52979.64149	···	···	···	< 21.05
52982.71623	···	···	···	< 19.80
52985.24459	···	20.95 (0.03)	···	···
52986.27416	···	20.81 (0.03)	···	···
52988.68744	···	···	···	20.21 (0.18)
52988.28817	···	20.24 (0.02)	···	···
52990.25875	···	19.83 (0.02)	···	···
52992.29069	···	19.82 (0.03)	···	···
52992.73489	···	···	···	19.65 (0.10)
52994.31115	···	19.81 (0.02)	···	···
52996.28857	···	19.87 (0.02)	···	···
52997.44242	···	···	···	19.77 (0.09)
52998.25951	···	19.95 (0.02)	···	···
53000.31187	···	20.03 (0.02)	···	···
53001.72660	···	···	···	19.83 (0.08)
53004.32118	···	20.12 (0.02)	···	···
53011.28573	···	···	···	19.92 (0.10)
53019.31815	···	20.23 (0.02)	···	···
53029.29812	···	···	···	19.90 (0.04)
53052.97253	···	···	···	19.91 (0.05)
53077.45696	···	···	···	20.02 (0.05)
53106.03597	···	···	···	20.53 (0.07)
53257.38920	···	22.02 (0.05)	···	···
53268.26639	23.15 (0.17)	···	···	···
53268.27047	···	···	21.15 (0.06)	···
53285.33774	···	···	···	21.05 (0.07)
53289.21636	···	22.22 (0.06)	···	···
53295.33515	···	22.08 (0.06)	···	···
53297.22518	···	22.18 (0.06)	···	···
53299.36194	···	22.15 (0.06)	···	···
53299.36544	23.34 (0.40)	···	···	···
53299.36742	···	···	21.13 (0.10)	···
53315.28817	···	22.08 (0.06)	···	···
53325.24440	···	22.12 (0.06)	···	···
53329.29664	···	22.17 (0.06)	···	···
53331.34066	···	22.11 (0.06)	···	···
53348.18819	···	22.20 (0.06)	···	···
53350.32545	···	22.17 (0.07)	···	···
53352.23171	···	22.21 (0.06)	···	···
53354.23758	···	22.18 (0.06)	···	···
53356.25495	···	22.16 (0.07)	···	···
53404.63460	···	···	···	21.30 (0.12)
53414.22055	···	22.11 (0.06)	···	···
53639.30253	···	22.77 (0.10)	···	···
53641.33128	···	22.60 (0.12)	···	···
53649.38498	···	22.68 (0.11)	···	···
53652.32054	···	22.81 (0.11)	···	···
53654.22569	···	22.68 (0.10)	···	···
53663.32678	···	···	···	21.24 (0.08)
53684.22316	···	22.67 (0.09)	···	···
53704.30592	···	22.65 (0.09)	···	···
53706.22709	···	22.56 (0.10)	···	···
53712.35217	···	22.69 (0.12)	···	···
53714.35882	···	22.69 (0.29)	···	···
53733.16559	···	22.62 (0.08)	···	···
53738.16874	···	22.71 (0.09)	···	···
53777.61556	···	···	···	21.39 (0.10)
54006.82171	···	···	···	21.87 (0.20)
54127.67356	···	···	···	21.46 (0.14)
54402.73904	···	···	···	22.26 (0.22)
54502.13612	···	···	···	22.47 (0.23)
54674.41064	···	23.82 (0.41)	···	···
54674.42468	···	···	22.61 (0.45)	···
54704.35730	···	24.19 (0.20)	···	···
54704.37563	···	···	22.59 (0.15)	···

2 – 9 (epoch 2) for its MIPS observations. We used the epoch 1 and 2 images provided by the *SAGE* team to produce small (300 pixel wide) cutouts around the position of SN 2003ma, for all four IRAC bands and the 24 μm MIPS band. The IRAC and MIPS cutouts have spatial scales of 1.2 and 2.5 arcsec pixel^{-1}, respectively, and are all on a common coordinate reference frame.

Although an object was clearly visible at the position of SN 2003ma on several of the *Spitzer* images, we found that the *SAGE* catalog did not contain photometry for it in all bands, likely due to the presence of several bright stars near the SN 2003ma position. Moreover, because the crowding in the *Spitzer* images forced us to conduct artificial star tests in order to understand the true photometric errors, we performed our own PSF-fitting photometry on the image cutouts using DAOPHOT/ALLSTAR (Stetson 1987). We used a threshold of 1σ to find stars and a sequence of apertures for initial photometry. To derive a PSF for each image, we first selected 30 – 130 PSF stars for the IRAC images, and 18 for the MIPS 24 μm image. We then used an iterative procedure of fitting a PSF function to the PSF stars, subtracting neighboring sources, and then refitting the PSF function to the PSF stars, while increasing the order of the spatial variability of the function up to a maximum of two. After several iterations, we used the derived PSF to derive photometry for all detected sources. After subtracting all sources except for the PSF stars, we calculated aperture photometry of the PSF stars out to a radius of 11 pixels ($13\farcs2$) for the IRAC images, and 29 pixels ($72\farcs5$) for the MIPS 24 μm images. We used this aperture photometry to apply a correction to the PSF-fitted photometry. Finally, we matched the aperture-corrected photometry to that of sources in the *SAGE* catalog, and applied the zero-point differences to provide the photometric calibration.

For three of the images (epochs 1 and 2 for the 3.6 μm band, and epoch 1 for the 4.5 μm band), we found that the crowding in the images and the intrinsic faintness of the object left SN 2003ma still unmeasured, with no matching sources within 3 pixels of its position. For these three images, we thus use the 8.0 μm epoch 1 image positions as the master source list, and forced ALLSTAR to fit photometry at the positions, allowing only the sky and object magnitude to be free parameters.

To ensure that our derived photometric uncertainties were reasonable in the *Spitzer* images which all suffer from crowding, we performed artificial star tests. Artificial stars were added, a few at a time, to copies of the original images, measured using the photometric procedure described above, and then analyzed to evaluate the photometric errors, offsets, and completeness as a function of input magnitude. In the course of these tests, we added a total of 10,000 artificial stars, with magnitudes distributed evenly over the range $14 \leq M_{3.6\ \mu\mathrm{m}} \leq 18$ mag, and with colors with respect to the other bands matched to those observed for SN 2003ma. The stars were added 50 at a time ($\sim$5% of the real detected sources in each image) at random positions. Following the photometric measurement step, we recovered the detected artificial stars by first removing from the output lists all stars matching real sources detected in the original images, and then comparing the remaining sources with the list of input artificial stars. We then computed the average offset and dispersion in the input minus recovered magnitudes and the fraction of artificial stars recovered as a function of input magnitude.

Table 2 lists the *Spitzer* photometry of SN 2003ma, and the quantities derived from the artificial star tests. The measured flux in mJy is shown in the 3rd column. The flux uncertainty in the 4th column was determined by DAOPHOT and is typically between 5% - 15%. This is the appropriate relative uncertainty between the fluxes measured in the same band but different epochs, since any bias due to crowding should have nearly the same effect in both epochs assuming that the neighboring objects are not variable. For different wavelengths, the crowding is different and thus has a different impact on the photometry. Therefore our estimate for the total photometric uncertainty (6th column in Table 2) of SN 2003ma at each epoch is based on the mean photometric uncertainty arrived at in the appropriate magnitude range of the artificial stars lists. For all comparisons of fluxes from different bands, we use these total errors, which are $\sim$30%, $\sim$30%, $\sim$30 – 50%, $\sim$10 – 15%, and $\sim$20% for the 3.6, 4.5, 5.8, 8.0, and 24 μm images, respectively.

The average absolute offsets in the input minus recovered magnitudes of the artificial stars are typically smaller than 0.1 mags, such that we do not expect the Spitzer detections of SN2003ma to be spurious. The only exception is the 5.8 micron photometry, for which the absolute offsets are 0.5 mags. The average completeness for the 5.8 μm images at the magnitude of SN 2003ma was also <50%, which suggests that the 5.8 μm photometry is unreliable compared to that in the other bands. As a consistency check, we compared our unforced photometry to the recently complete, final catalog and archive lists from the *SAGE* project (Meixner et al. 2006) and found them to be in agreement.

2.3. *Spectroscopy*

We followed SN 2003ma spectroscopically for nearly six years using the 8 m Gemini-South telescope (with GMOS; Hook et al. 2004) and the 6.5 m Magellan Clay telescope (with LDSS2; Allington-Smith et al. 1994, LDSS3[30], and MagE; Marshall et al. 2008). The spectra[31] are presented in Figure 5 and a journal of observations are presented in Table 3.

Standard CCD processing and spectrum extraction were accomplished with IRAF. The data were extracted using the optimal algorithm of Horne (1986). Low-order polynomial fits to calibration-lamp spectra were used to establish the wavelength scale, and small adjustments derived from night-sky lines in the object frames were applied. For the MagE spectrum, the sky was subtracted from the images using the method described by Kelson (2003). We employed our own IDL routines to flux calibrate the data and remove telluric lines using the well-exposed continua of the spectrophotometric standards (Wade & Horne 1988; Foley et al. 2003, 2009).

The 2004 spectrum was obtained far from the parallactic angle at high airmass. As a result, its continuum and

[30] http://www.lco.cl/telescopes-information/magellan/instruments-1/ldss-3-1/ .

[31] The Gemini South GMOS spectra were obtained as part of the GS-2003B-Q-12 science program and the header target name in the images and spectra was cand10194.sm76_4.

TABLE 2
IRAC and MIPS Photometry and Artificial Star Test Results

Band (μm)	t[a]	Flux[b] (mJy)	Flux relerr[c] (mJy)	ΔFlux[d] (mJy)	Flux err[e] (mJy)	Compl.[f] (%)
3.6	1	0.063[g]	0.006	0.006	0.018	46.4
4.5	1	0.048[g]	0.003	0.003	0.014	53.3
5.8	1	0.059	0.004	0.017	0.017	38.9
8.0	1	0.108	0.004	0.014	0.018	77.3
24.0	1	1.164	0.080	0.099	0.227	94.4
3.6	2	0.055[g]	0.003	0.005	0.019	40.9
4.5	2	0.065	0.003	0.006	0.014	65.6
5.8	2	0.028	0.004	0.015	0.013	13.6
8.0	2	0.184	0.006	0.014	0.022	89.3
24.0	2	1.141	0.108	0.098	0.228	94.0

[a] Epoch ID. Epoch 1 spans from 2005 July 15 – August 3, and epoch 2 from 2005 October 26 – November 9.
[b] Flux at the position of SN 2003ma. This flux contains both the flux of SN 2003ma as well as any potential flux from the host galaxy.
[c] Flux error as determined by DAOPHOT. This is the appropriate relative error between the fluxes measured in the same band at different epochs
[d] Average detected flux minus input flux as derived from artificial star tests, interpolated at the measured flux level of SN 2003ma in each image.
[e] Average dispersion in the detected flux minus the input flux from the artificial star tests, interpolated at the measured flux level of SN 2003ma in each image.
[f] Average completeness in %.
[g] Forced photometry.

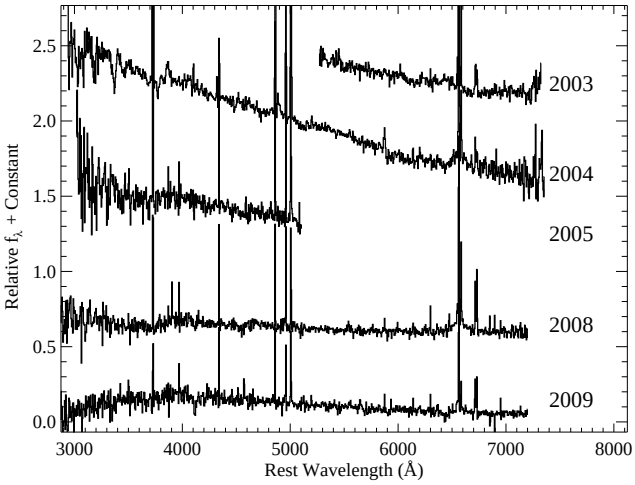

Fig. 5.— Optical spectra of SN 2003ma. The spectra are denoted by the year in which they were obtained. The spectra in years 2003, 2004, 2005, and 2008 correspond to rest-frame phases of 1, 279, 905, and 1423 days relative to B maximum, respectively. There is significant galaxy contamination in all spectra, likely dominating the spectrum at later phases. Since the 2004 spectrum was not obtained at the parallactic angle, its spectral shape is likely incorrect.

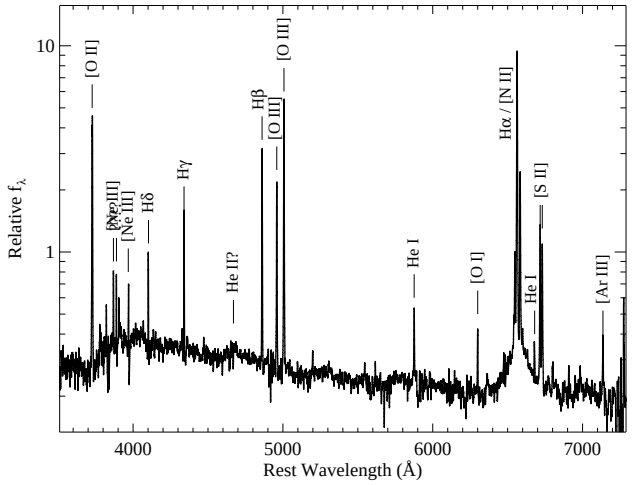

Fig. 6.— Optical spectrum of SN 2003ma from 2008 (t = 1423 days). Narrow emission lines are marked. The continuum is likely dominated by the host galaxy, while the broad Hα and potential He II λ4686 lines are from SN 2003ma.

TABLE 3
Log of Spectral Observations

Phase[a]	UT Date	Telescope / Instrument	Exposure (s)
1	2003 December 22.3	Gemini South/GMOS	3×610
279	2004 December 14.1	Magellan/LDSS2	1500
905	2005 October 29.3	Magellan/LDSS3	900
1423	2008 December 28.3	Magellan/MagE	2×1800
1649	2009 October 17.3	Magellan/MagE	1800, 1200

[a] Rest-frame days since B maximum, 2003 December 20.8 (JD 2,452,994.3).

any derived line ratios are likely incorrect (Filippenko 1982). Since the offset between the SN and host is very small, we were not able to perform local galaxy subtraction during extraction. For the 2003 and 2008 spectra, we have calibrated our absolute spectrophotometry to match concurrent photometry of the SN and host combined. This is not possible for the 2004 and 2005 spectra because of incorrect relative spectrophotometry and a small wavelength range that does not fully cover any of our broad-band filters, respectively.

Several narrow galactic emission lines are present in all spectra and are identified in Figure 6 at a redshift of $z = 0.289$. Throughout this paper we assume a cosmology with $H_0 = 70$ km s^{-1} Mpc^{-1}, $\Omega_m = 0.3$, $\Omega_\Lambda = 0.7$, which yields a luminosity distance of $d_L = 1486$ Mpc for the SN redshift.

3. COMPARISONS TO OTHER CORE-COLLAPSE SUPERNOVAE

3.1. *Spectroscopic Comparisons*

The five spectra of SN 2003ma are presented in Section 2.3. The 2008 and 2009 spectra are dominated by host-galaxy light (see Figure 6); however, there is a strong, broad component to the Hα line. We are confident that this broad component is from the underlying SN and not from another source such as an AGN (for instance, the broad component is not visible in our 2003 spectrum).

The 2003 spectrum is much bluer than the late-time spectra, indicating that it contains more SN light than the late-time spectra, which is not surprising considering that the SN was $\sim$3 mag brighter in 2003 compared to 2008. In order to isolate the SN continuum in the 2003 spectrum, we have subtracted a galaxy template spectrum from the 2003 spectrum. We chose the galaxy template to match the general continuum shape of the late-time spectra. The pre-event photometry can be used to properly scale the galaxy template. Similarly, the photometry at the time of each SN spectrum can be used to scale each spectrum. Unfortunately, this procedure produces a galaxy spectrum that is $\sim$10% too bright compared to the late-time spectrum (assuming that the late-time spectrum is dominated by the host galaxy). However, considering the fact that the galaxy template spectrum does not include emission lines and there may be crowding in the template image, we do not consider this to be a significant discrepancy. The galaxy template spectrum was rescaled to match the continuum of the 2008 spectrum and subtracted from both the 2003 and 2008 spectra.

We present the dereddened (our spectra of SN 2003ma have only been corrected for foreground extinction based on Galactic dust maps Schlegel et al. 1998; see Section 4.1) galaxy-subtracted 2003 and 2008 spectra in Figure 7. We compare these spectra to those of SN 2005ip (Smith et al. 2009b), after dereddening the spectra of SN 2005ip by $E(B-V) = 0.047$ mag to account for Milky Way extinction. In order to match the continuum slope of SN 2003ma, we add an additional $E(B-V) = 0.9$ mag of host extinction. Smith et al. (2009b) found that SN 2005ip may have had host extinction of $E(B-V) = 0.3$ mag based on measurements of Na D absorption, however since the absorption features were only clearly detected in the spectrum taken 1 day after discovery, they were unsure of the true magnitude of extinction. It seems unlikely that SN 2005ip suffered from $E(B-V) = 0.9$ mag of reddening without strong Na D absorption. Instead, the difference in continuum shapes may indicate that SN 2003ma was hotter at this epoch than SN 2005ip (see also Section 4.2).

At maximum, both SN 2003ma and SN 2005ip have relatively featureless continua. With the applied extinction corrections, there are no significant deviations between the two spectra. The spectrum of SN 2003ma is consistent with that of a blackbody. There is a low amplitude, broad feature in the SN 2003ma spectrum at $\sim$6150 Å(in the rest frame) that may correspond to Hα absorption. If this identification is correct, the feature would have an absorption minimum blueshifted by $\sim$20,000 km s^{-1}. In Figure 7, we also compare the 2008 spectrum of SN 2003ma to the $t = 905$ day spectrum of SN 2005ip (Smith et al. 2009b). The continua of the spectra match, but this may be the result of an incorrect treatment of the galaxy contamination. The only feature of significance is the Hα line, which is much broader for SN 2003ma compared to SN 2005ip. The broad Hα line is also seen in the 2009 spectrum, but at lower equivalent width.

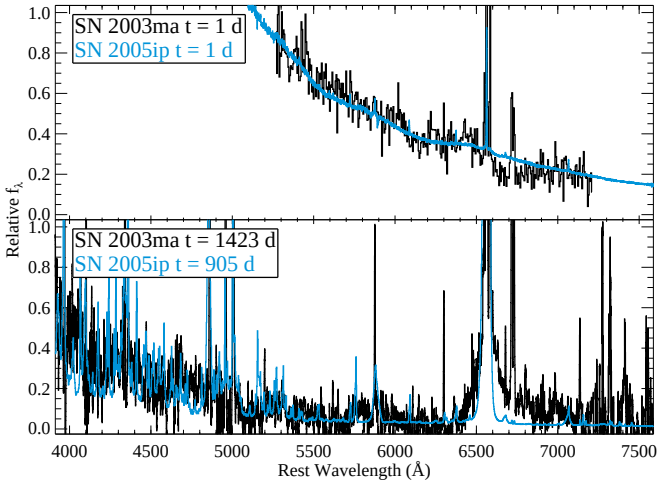

FIG. 7.— Optical spectra of SN 2003ma compared with those of SN 2005ip. Phases are given in rest-frame days since maximum light. Top: Galaxy-template subtracted maximum-light spectrum of SN 2003ma (black) and maximum-light spectrum of SN 2005ip (blue). An additional E(B-V)=0.9 mag of internal extinction was applied to SN 2005ip to match the continuum shape of SN 2003ma. Bottom: The 1423 day (4 year; black) and 905 day (2.5 year; blue) spectra of SN 2003ma and SN 2005ip, respectively. A template galaxy spectrum has been added to the SN 2005ip spectrum to match the continuum shape of the SN 2003ma spectrum.

We detect narrow He I λ5876 emission in the spectra from 2004, 2008, and 2009, but do not detect it in the 2003 spectrum (the wavelength range of the 2005 spectrum does not cover this feature). The 2003 spectrum has a relatively low S/N, and the He I may be too weak to be detected. Alternatively, in Section 4.2, we argue that the blackbody temperature in 2003 was $\gtrsim 15,000$ K, which should produce sufficient high-energy photons to singly ionize He. In Figure 6, we tentatively identify relatively broad He II λ4686 in the 2008 spectrum. If correct, this would require a significant amount of ionizing far-UV or X-ray photons from the circumstellar interaction to ionize He in the post-shock material. However, as shown in Figure 7, SN 2005ip has several narrow lines in this region of the spectrum. It is possible that the 2008 spectrum of SN 2003ma does not have a high enough S/N to see these individual lines.

In SNe IIn, the Hα line can have up to four distinct components: broad, intermediate, narrow, and galactic. Smith et al. (2009b) was able to identify the first three regions for SN 2005ip, while the fourth component was not seen. Physically, the broad, intermediate, and narrow components are formed in the fast-moving SN ejecta, the post-shock circumstellar material, and the pre-shock circumstellar material, respectively. The widths of the broad and narrow components indicate the velocity of the SN ejecta and the circumstellar wind/ejection, re-

spectively, while the intermediate component is an indication of the amount of energy transferred from the shock to the circumstellar material. The galactic component, which is the line-of-sight emission from the host galaxy and physically unrelated to the SN, may have a similar velocity to that of the narrow component.

In Figure 8 we show the narrow [O I] λ6300, Hα, [N II] $\lambda\lambda$6548, 6583, and [S II] $\lambda\lambda$6716, 6731 emission lines fitted with a Voigt profile with its width fixed to that of the [N II] λ6583 line in each spectrum. The Voigt profile produces better fits to the wings of the narrow lines than a single Gaussian. The narrow lines are unresolved in the 2003 and 2004 spectra, but the high resolution of the 2008 and 2009 spectra resolves the narrow lines to have a FWHM = 110 km s^{-1}. In 2004, 2008, and 2009 we fit the broad base beneath the Hα+[N II] narrow-line complex with a Gaussian. The best fit was for a Gaussian with FWHM = 5800 ± 800 km s^{-1} and a velocity offset of +350 km s^{-1} relative to the narrow Hα line. This velocity offset could be due to asymmetries in the line profile. The broad component is not detected in the 2003 spectrum, and we place an upper limit on the presence of this Gaussian component to be < 0.2 times the flux of the narrow Hα line. The ratio of the broad component to the narrow component of Hα is 0.7 ± 0.1, 0.4 ± 0.2, and 0.5 ± 0.2 in 2004, 2008, and 2009, respectively. The change in this ratio is not statistically significant, and systematic effects such as different position angles of the slit and varying seeing can also produce differences.

We measure the standard diagnostic [O III]/Hβ and [N II]/Hα, and [S II]/Hα narrow-line ratios (Baldwin et al. 1981; Veilleux & Osterbrock 1987), which are insensitive to extinction and atmospheric refraction, for each spectrum from the Voigt profile fits. The narrow-line ratios, listed in Table 4, are all consistent with a star-forming galaxy. This, in combination with the lack of variability in the densely sampled SuperMACHO and OGLE difference imaging data over a baseline of 7 years before the SN, place strong constraints on the presence of an AGN in the host galaxy.

If the broad Hα component is powered by CSM interaction, then we expect there to be some contribution to the narrow Hα and Hβ emission lines. However, with no observed velocity offset between the expected narrow component from the SN and the host galaxy emission lines, it is difficult to tell if the SN contributes to the narrow emission lines. Furthermore, the narrow-line ratios are measured to be constant within the errors from 2003 to 2008, and thus the lines are most likely dominated by the H II regions in the host galaxy. The luminosity of the Hα line in 2003, when the broad component of Hα associated with the SN is not yet observed, is $L(H\alpha) = 6.1 \times 10^{42}$ ergs s^{-1}, which corresponds to a substantial star-formation rate of $4.8 M_{\odot}$ year^{-1} characteristic of a starburst galaxy (Kennicutt 1998).

At day 905, SN 2005ip had been on its plateau for over 2 years, and the broad component of its Hα line had faded by a factor of $\sim$6 while its narrow+intermediate Hα line, which is assumed to be powered by interaction with the CSM, had increased by a factor of 3, resulting in a nearly constant total Hα luminosity (Smith et al. 2009b). At this epoch, the FWHM of the intermediate component and broad component of Hα were 740 ± 250 km s^{-1} and 8800 ± 660 km s^{-1}, respectively (Smith et al. 2009b). In comparison, at day 279 and 1423, SN 2003ma was on its second plateau and also most likely dominated by circumstellar interaction, however the width of the broad component of its Hα line is at least 5 times larger than the intermediate component seen in SN 2005ip. Similarly, it is significantly broader than the intermediate component of Hα observed in SNe IIn 1988Z, 2006tf, and 2007rt which had a characteristic width of 2000 km s^{-1} (Aretxaga et al. 1999; Smith et al. 2008a; Trundle et al. 2009) and SN 2006gy which had an intermediate component with 4000 km s^{-1} (Smith et al. 2007b).

The $\sim$6000 km s^{-1} component seen in the 2004 and 2008 spectra of SN 2003ma could be associated with SN ejecta that has decelerated over time. The width of the broad component of Hα was observed to decrease from $\sim$15,000 km s^{-1} on day 34 to 5000 km s^{-1} after day 500 in SN 1988Z (Aretxaga et al. 1999) and decrease from $\sim$10,000 km s^{-1} on day 102 to < 6000 km s^{-1} after day 273 in SN 2007rt (Trundle et al. 2009). It may be that the day 1 spectrum of SN 2003ma was too early, and the day 279 spectrum was too late to catch the broad component when it had a velocity width of tens of thousands of km s^{-1}. However, given the long-lived plateau in the light curve, circumstellar interaction must be the dominant source of energy after day 90. Thus, the broad component in SN 2003ma is most likely an exceptionally fast "intermediate component" that is the result of the interaction with the CSM of a highly energetic explosion, even more energetic than SN 2006gy (see Section 4.5), which imparts a much faster blast-wave speed to the postshock shell. However, electron scattering can also be a significant source of broadening of the Hα line in interacting SNe, and thus the speed of the material may be slower than inferred from the width of the line (Dessart et al. 2009).

3.2. *Photometric Comparisons*

The I-band light curve of SN 2003ma has two nearly flat plateaus, and strong emission in the V and I bands for $\sim$1000 days, reminiscent of the long-lived emission seen in interacting SNe IIn. Although the first plateau in the rest-frame R-band is similar to the initial plateau seen in SNe IIP, its comparable plateau in the rest-frame B band is unlike IIP SNe which begin their decline immediately after the peak in the B band. Figure 11 shows a comparison of SN 2003ma to canonical SN IIP 1999em (Leonard et al. 2002; Elmhamdi et al. 2003), along with extreme interacting SNe IIn 1988Z (Aretxaga et al. 1999) and 2005ip (Smith et al. 2009b), and extremely luminous SN IIn 2006gy (Ofek et al. 2007; Smith et al. 2007b), SN IIL 2005ap (Quimby et al. 2007), SN IIL 2008es (Miller et al. 2009; Gezari et al. 2009a), and normal SN Ia 1988aq (Riess et al. 2005). All light curves are corrected for Galactic extinction, and in the case of SN 1999em and SN 2006gy for internal extinction (Leonard et al. 2002; Smith et al. 2007b). K-corrections are applied to SNe at distances farther than 100 Mpc.

In SNe IIP, a plateau is observed in the V and R bands as a result of H recombination in the SN ejecta. The plateau is not seen at shorter wavelengths (U and B

TABLE 4
Diagnostic Narrow-Line Ratios

Year	[OIII]λ5007/Hβ	[NII]λ6583/Hα	[SII]$\lambda\lambda$6716, 6731/Hα
2003	1.98 ± 0.07	0.18 ± 0.01	0.21 ± 0.02
2004	2.19 ± 0.03	0.23 ± 0.04	0.21 ± 0.03
2005	2.10 ± 0.07	...	...
2008	2.19 ± 0.05	0.22 ± 0.02	0.18 ± 0.01
2009	1.71 ± 0.12	0.19 ± 0.02	0.17 ± 0.01

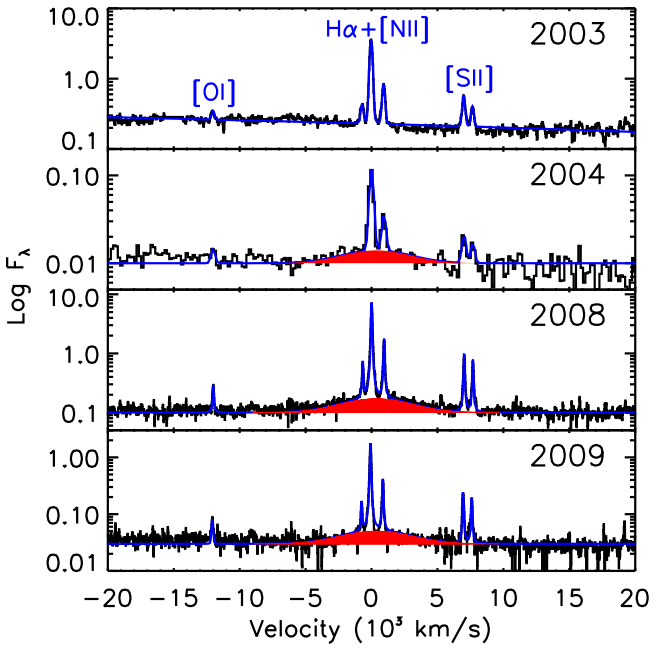

Fig. 8.— Narrow [O I] λ6300, Hα, [N II] $\lambda\lambda$6548, 6583, and [S II] $\lambda\lambda$6716, 6731 emission lines fitted with Voigt profiles with a width equal to the [N II] λ6583 line in each spectrum, respectively, are shown with a blue line. In 2003 the continuum if fitted with a quadratic function, and in 2004, 2008, and 2009 the continuum is fitted with a constant value. An additional broad Gaussian component that is needed to fit the Hα line in 2004, 2008, and 2009 is shown in red. In 2004 the [N II] λ6548 line is not detected above the noise, and is weaker than expected for a line ratio of 3:1 for [N II] λ6583/λ6548.

bands) due to sensitivity to the declining temperature and line blanketing from metals, nor at longer wavelengths (I band) since the bandpass is on the Rayleigh-Jeans tail of the emission the whole time (Leonard et al. 2002).

The SuperMACHO data constrains the pre-maximum light curve of SN 2003ma exceedingly well (see Figure 12). The first significant detection is 4.5 mag below peak 20 days before maximum, and we estimate the day of explosion to be between the last upper limit and the first detection at t_0 = MJD 52,971 ± 1. The slow decline of the I band (rest-frame R band) in the first plateau (53010 ≤ MJD < 53110 or $t - t_0$ = 40 − 140 days) of 0.0017 ± 0.0009 mag day^{-1} and in the second plateau (MJD ≥ 53110 or $t-t_0$ = 140−1735 days) of 0.0011±0.0001 mag day^{-1} is much flatter than the 481 day decline seen in SN IIn 2007rt with 0.006 mag day^{-1} (Trundle et al. 2009), and is more like the extreme plateaus observed in the light curves of SNe IIn 1988Z and 2005ip (see Figure 12). The slow decline in these SNe IIn light curves are explained by an excess of emission above the photospheric emission produced by the interaction of the SN ejecta with circumstellar material. The spectra of these SNe demonstrated broad Balmer emission lines, with a narrow component and no P-Cygni absorption, suggesting that the emission is confined to an outer shell (Turatto et al. 1993).

The color evolution of SN 1988Z and SN 2003ma, shown in Figure 13, are remarkably similar. The extremely flat plateaus of this type of SN are attributed to an increase in narrow and intermediate-width Hα flux as well as a forest of other narrow lines powered by the circumstellar interaction (Smith et al. 2008a). The decreasing Hα line velocity width over time in SN 1988Z was successfully modeled by Aretxaga et al. (1999) as the consequence of a SN remnant shock expanding into a dense medium. The fact that SN 2003ma is bluer than SN 1988Z in particular during the early phases can be attributed to the higher blackbody temperature.

4. PHYSICAL PARAMETERS OF SN 2003ma

4.1. *Extinction*

We use the typical galactic extinction law of Cardelli et al. (1989) parameterized by a value of $R_V = A_V/E(B-V) = 3.1$. We obtain[32] a combined Galactic and LMC reddening of $E(B-V) = 0.348$ mag at the position of SN 2003ma from Schlegel et al. (1998). As a consistency check, we examine the spectra of SN 2003ma for tracers of interstellar dust. The Na D doublet is not detected at or near zero velocity in any of our spectra. The 2008 spectrum of SN 2003ma, which has a resolution of ∼20 km s^{-1}, is ideal for examining the Na D doublet. We present the wavelength regions from that spectrum which correspond to the rest-frame Na D doublet for the Milky Way, LMC, and host galaxy of SN 2003ma in Figure 9. From this spectrum, we can rule out Na D absorption with an equivalent width of $\gtrsim$ 0.4 Å from the Milky Way and the LMC. Using the relationship of Barbon et al. (1990), we expect $E(B-V) \lesssim 0.1$ mag from the Milky Way and the LMC, respectively. However, Blondin et al. (2009) found $E(B-V) > 0.3$ mag for objects with Na D equivalent widths below about 0.3 Å. We therefore believe that our measurements of Na D are consistent with the Schlegel et al. (1998) extinction estimates.

In Figure 9, we see that there is a possible detection of Na D absorption from the host galaxy at a redshifted velocity of $v = 200$ km s^{-1} relative to the host galaxy with a width of $\lesssim 20$ km s^{-1}, the resolution of our spectrum. However, we do not see a narrow emission line component from the SN that is offset from the emission lines of

[32] http://irsa.ipac.caltech.edu/applications/DUST/

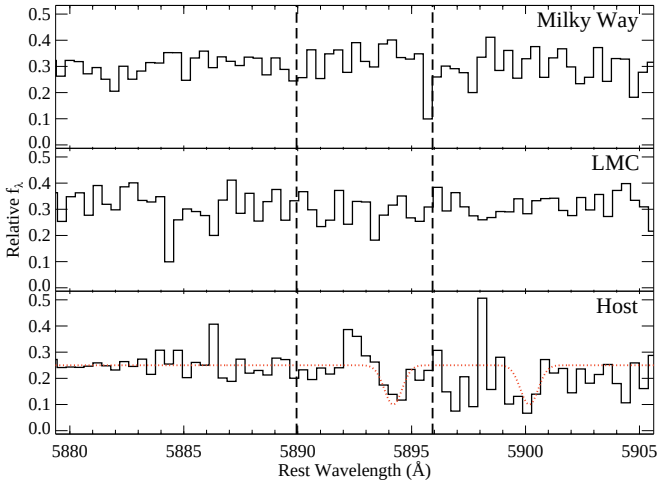

FIG. 9.— Optical spectrum of the 1423 day spectrum of SN 2003ma near the rest wavelength of the Na D doublet for the Milky Way (top), LMC (middle), and host galaxy (bottom), respectively. The vertical dashed lines indicated the wavelengths of the Na D lines. We detect no Na D absorption in the Milky Way or LMC to a equivalent width limit of ∼0.4 Å. There is the possibility of Na D absorption in the host galaxy with a redshifted velocity of 200 $\mathrm{km\,s^{-1}}$ relative to the host galaxy with an equivalent width of 0.5 Å. This possibility is represented by the red dashed lines.

the host galaxy. There are three possible explanations for the lines. First, the lines could be a spurious detection caused by random noise. This is plausible given the level of noise in the spectrum and the slightly odd line profiles. Second, there could be an absorbing cloud traveling toward SN 2003ma. SN 2003ma is at the same redshift as its host galaxy; therefore, SN 2003ma (either in a disk or the halo) would have its velocity vector pointing mostly perpendicular to our line of sight. If the cloud is in the disk, then SN 2003ma must be in the halo, and likewise, if SN 2003ma is in the disk, then the cloud must be in the halo. Third, there is local material falling inward towards SN 2003ma. Either circumstellar material or gas from an H II region may be under gravitational collapse, however the velocity appears to be very high for such a scenario. Given the possibilities, we believe the most plausible is that there is no significant Na D absorption near the redshift of the host galaxy, which indicates no additional extinction from the host galaxy. However, the fact that there is a strong IR echo (see Section 4.8) in combination with the type of the host galaxy being a star-forming galaxy which are generally dust-rich, makes it very likely that there is significant extinction in the host. The lack of Na D absorption might then be due to bleaching of the Na D doublet out to a few hundred pc by photoionizing Na I to Na II. Considering all these circumstances we assume as a lower limit no additional extinction from the host galaxy throughout the paper. Consequently, the total assumed $E(B-V) = 0.348$ mag is also a lower limit. Any additional extinction beyond the Milky Way Galaxy and LMC foreground component increases the required SN luminosity and hence makes the SN even more extreme in its characteristics.

For each passband, we compute the combined Galactic and LMC extinction at its effective wavelength $\lambda_{\rm eff}$ with $A(\lambda_{\rm eff}) = \langle A(\lambda_{\rm eff})/A_V \rangle\, E(B-V) R_V$ using Equation 1 from Cardelli et al. (1989). Table 5 shows the effective wavelengths and extinction for the various passbands in the second and third column, respectively.

4.2. *Temperature at Peak*

As described in Section 3.1, we obtained a spectrum of the event and host galaxy on 2003 December 22, ∼3 days after peak. To examine the temperature of this spectrum, we focus on the dereddened, galaxy-subtracted spectrum (see Section 3.1 and Figure 7). We ignore the region of the spectrum corresponding to 6350 – 6800 Å in our analysis below to avoid any Hα contamination. The spectrum shows a blue continuum without any significant emission or absorption lines. This is similar to the spectra of SNe II caught within days of explosion which also show a relative featureless blue continuum which can be fitted with blackbody temperatures of ∼10,000 – 20,000 K (e.g., Dessart & Hillier 2006; Dessart et al. 2008; Gezari et al. 2009a). The earliest spectrum of SN 2005ip also demonstrates a blue, featureless continuum on day 1 after discovery that is fitted with a blackbody with $T_{\rm BB} = 7300$ K; however, this temperature is most likely a lower-limit due to the uncertainty in the amount of internal extinction (Smith et al. 2009b).

Figure 10 shows the 2003 galaxy-subtracted spectrum of SN 2003ma (black line), in comparison to black bodies of 5000, 10,000, 15,000, and 20,000 K. In order to further constrain the blackbody fit, we use the observed broadband fluxes in $VR_{\rm SM}$ and $I_{\rm OGLE}$ (blue square and red diamond). The horizontal error bars indicate the width of the filters. Black bodies with $T \lesssim 10,000$ K do not fit well (see solid orange line and dashed sky blue). For higher temperatures, a differentiation is not possible since the observed wavelength range only covers the Rayleigh-Jeans tail of the blackbody. Therefore we can only set a lower limit of the temperature at peak of $T_{\rm peak} \gtrsim 15,000$ K.

4.3. *Absolute Magnitudes*

We calculate the absolute magnitude M_X in the rest-frame filter X from an observed magnitude m_Y in filter Y as

$$M_X = m_Y - A_Y - DM - K_{XY} \qquad (1)$$

where A_Y is the extinction in filter Y as described in Section 4.1, DM is the distance modulus and K_{XY} is the K-correction. For a redshift of $z = 0.289$, we compute $DM = 40.86$ mag. At this redshift, the filters B, VR, and I in the observers frame are best matched by the rest-frame filters U, B, and R, respectively. The K-correction K_{XY} as well as the bolometric correction described in the next section depend on the choice of the spectral energy distribution (SED) used to represent the SN SED. Due to the limited wavelength range of the observed spectra in addition to the imperfect background subtraction in particular for the later time spectra, we cannot use the SN 2003ma spectra to directly calculate the bolometric correction. Thus, we choose the following two SED models:

- **Solar model:** The solar spectrum is often used to estimate the bolometric correction. Although it does not necessarily represent the true underlying SED, it is commonly used in the literature for other

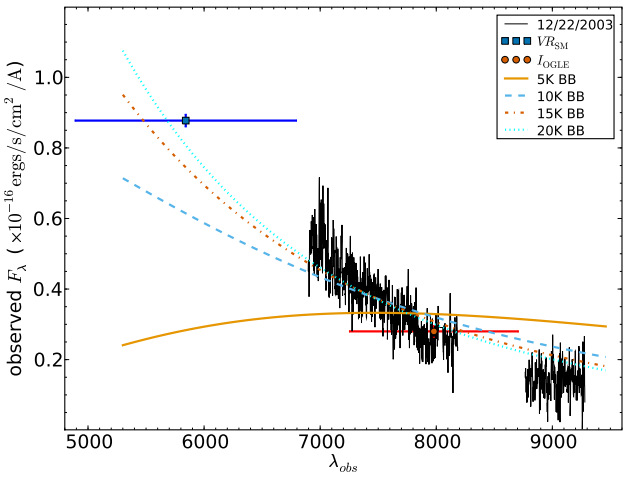

FIG. 10.— Spectrum of SN 2003ma (black line) from 2003 December 22 (∼3 days after peak) with galaxy contamination subtracted as discussed in Section 3.1 and dereddened. The galaxy Hα line does not fully subtract. Therefore the spectrum in the rest frame wavelength range 6350 – 6800 Å is not reliable and we do not use it in the analysis. Overplotted are the dereddened observed fluxes derived from the VR_{SM} (blue squares) and I_{OGLE} (red diamonds) photometry. The horizontal error bars indicate the width of the filters. The solid orange line, dashed sky blue line, dot-dashed purple line, and dotted cyan line indicate blackbody fits of 5000, 10,000, 15,000, and 20,000 K to the spectrum and photometry, respectively.

SNe, and thus it allows for a direct comparison to them.

- **BB15K/88Z model:** As we show in Section 4.2, the peak temperature is $T_{\rm peak} \gtrsim 15,000$ K. Thus we choose a 15,000 K blackbody as our SED during the peak (MJD $<$ 53010). Motivated by the fact that the light curves and color evolution of SN 2003ma are very similar to SN 1988Z after peak, we use the 6 April 1989 spectrum of SN 1988Z as the SED for the first plateau (53010 $\leq$ MJD $<$ 53110), and an average of three SN 1988Z spectra (corresponding to dates 18 April 1990, 20 February 1991, and 4 February 1992) for the second plateau (MJD $\geq$ 53110). The particular SN 1988Z spectra were chosen for their large wavelength coverage (4500 – 9000 Å) and high S/N.

While the solar SED is simple and should provide reasonable measurements, the BB15K/88Z model is the more physical model since it attempts to accurately describe the SN SED. The fifth column in Table 5 and the third through fifth columns in Table 6 show the K-corrections for the two models. Note that the differences between the K-corrections derived from the different models are a few tenths of a magnitude. Figure 11 and 12 show the absolute magnitude light curve of SN 2003ma (blue squares and red circles) derived assuming the solar SED for the K-corrections.

4.4. *Luminosity & Energy*

We derive the luminosity L_X of SN 2003ma in a passband X and its bolometric luminosity L by comparing it to the sun with

$$L_X = L_{\odot,X} 10^{-0.4(M_X - M_{\odot,X})} \quad (2)$$

$$L_{{\rm bol},X} = b_X L_X, \quad (3)$$

where b_X is the bolometric correction for band X. The solar luminosities $L_{\odot,X}$ are calculated with synthetic photometry off the solar SED (Lejeune et al. 1997) through Bessell passbands, and the solar magnitudes $M_{\odot,X}$ are taken from Colina et al. (1996). They are shown in the 6th and 7th column in Table 5, respectively. We combine $I_{\rm SM}$ and $I_{\rm OGLE}$ in all rest-frame measurements since they match well to the same rest-frame passband. We calculate the bolometric correction b_X for a filter X as the ratio of the bolometric luminosity of the reference SED with its luminosity in X, where the reference SED is defined by the model used (either solar model or BB15K/88Z model) and for the BB15K/88Z model also by its light-curve phase (see 8th column in Table 5 and 6th – 8th column in Table 6). Note that the bolometric luminosity $L_{{\rm bol},X}$ depends strongly on the bolometric correction and thus on the filter X. Since we have good light curves in rest frame B and R, we can get estimates of the bolometric luminosity from both light curves and then compare them. In addition, we add the luminosities in the rest frame B and R together (L_{B+R}), and estimate the bolometric luminosity $L_{{\rm bol},B+R}$ using a bolometric correction $b_{B+R}^{-1} = b_B^{-1} + b_R^{-1}$. Combining both filters decreases the systematic error since the overall corrections are smaller, as we discuss in Section 4.5.

For both the solar model and the BB15K/88Z model we estimate the amount of energy emitted in the rest frame B, R, and the combined $B+R$ passbands by integrating over time (see 10th and 9th column in Tables 5 and 6, respectively). The biggest source of systematic error is caused by the gap in the data in the rest frame B (observed frame VR) between 53020 $<$ MJD $<$ 53250, which contains the transition between plateau 1 and plateau 2 (see Figure 4). A simple linear interpolation over the gap may introduce a systematic overprediction of the flux. We estimate that this overestimate is smaller than 10%, and does not change our results. Note that the bolometric correction using the BB15K/88Z model is only pseudo-bolometric, since the SN 1988Z spectra used only have a finite wavelength range from about 4000 – 10,000 Å, not considering any contribution redward of the z band or blueward of the B band.

4.5. *Energy Emitted*

The upper left panel of Figure 14 shows the luminosities in the rest frame B, R and combined $B+R$ passbands using the solar SED for the determination of the K-correction. In the upper right panel, the same luminosities are shown, but using a 15,000 K blackbody SED for the K-correction during peak, and SEDs from SN 1988Z for the K-corrections during the plateau phase. The K-corrections for the two models are listed in Table 5 and 6. Note that the differences in K-corrections and thus luminosity are not bigger than 20%.

We estimate the total emitted energy in the different passbands by integrating over time (see solid lines in lower panels of Figure 14, and 10th and 9th column in Tables 5 and 6, respectively). For the solar model, the

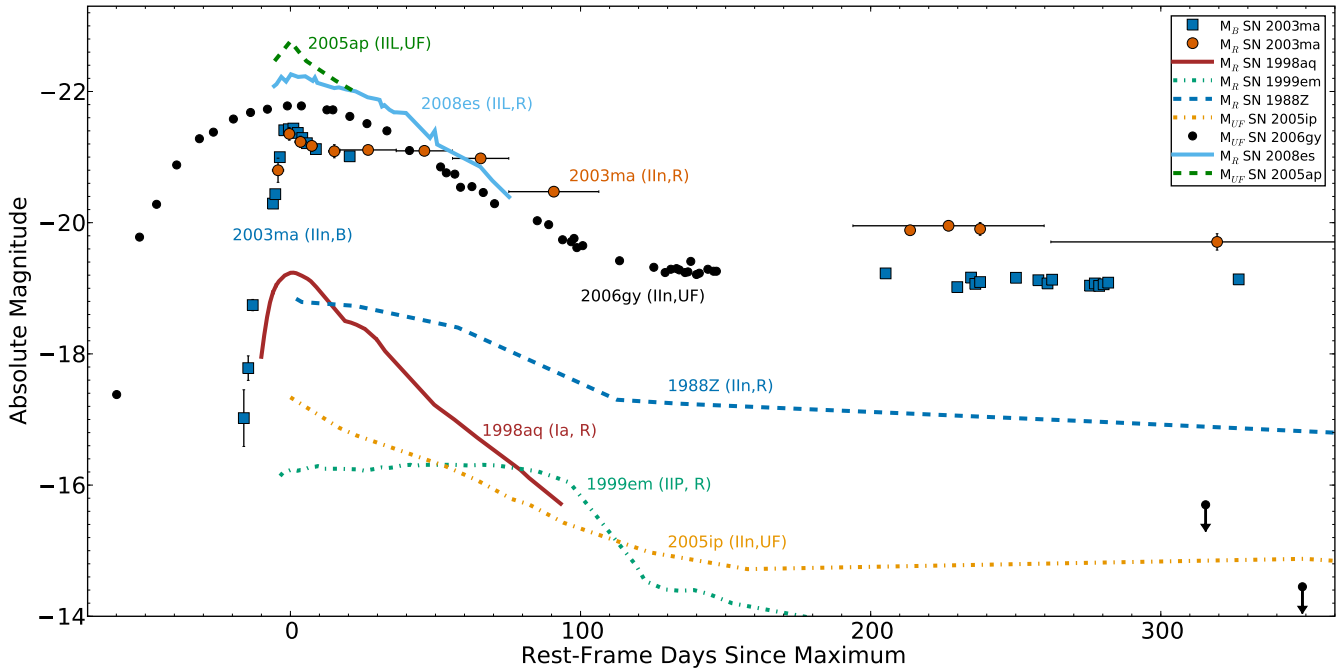

FIG. 11.— Light curve of SN 2003ma ($DM = 40.86$ mag, $z = 0.289$) in absolute, rest-frame B and R band magnitudes in comparison to SN IIn 1988Z ($DM = 34.77$ mag; Aretxaga et al. 1999), SN IIn 2005ip ($DM = 32.36$ mag; Smith et al. 2009b), the extremely luminous SN IIn 2006gy ($DM = 34.32$ mag; Smith et al. 2007b; Agnoletto et al. 2009), SN IIL 2008es ($DM = 40.08$ mag, $z = 0.21$; Miller et al. 2009; Gezari et al. 2009a), and SN IIL 2005ap ($DM = 40.81$ mag, $z = 0.283$; Quimby et al. 2007), SN Ia 1998aq ($DM = 31.696$, Riess et al. 2005), and SN IIP 1999em ($DM = 29.569$ mag; Leonard et al. 2002) in rest-frame days since maximum. The times of maxima for SNe 1998aq, 1999em, 2006gy, 2008es, and 2005ap are well constrained, but for SNe 1988Z and 2005ip there are no upper limits before the date of discovery, and so we assume that the date of discovery is the peak date. The light curves are in rest-frame B, R or R-like unfiltered (UF) magnitudes[a]. We do not apply any K-correction to the SNe with distances $\lesssim 100$ Mpc (SNe 1998aq, 1988Z, 1999em, 2005ip, and 2006gy). We convert the light curve of SN 2008es from observed i band to rest-frame R band by applying a K-correction of -0.043 mag. We convert the light curve of SN 2005ap from unfiltered magnitudes to rest-frame R band by applying a K-correction of 0.054 mag, assuming that the observed magnitudes are in R band. We apply extinction corrections of 0.036, 0.24, 0.126 and 1.78 mag to the light curves of SNe 1998aq, 1999em, 2006gy and 2005ip, respectively. The published light curves of SNe 1988Z, 2008es, and 2005ap are already extinction corrected. The observed VR and I-band measurements of SN 2003ma are extinction corrected by 0.66 and 1.01 mag, respectively, and then converted into rest-frame magnitudes in B and R bands with K-corrections of -0.63 and -0.51 mag, respectively. All K-corrections are calculated assuming a solar spectrum.

[a]The upper limits on the brightness of SN 2006gy are R band measurements from Agnoletto et al. (2009)

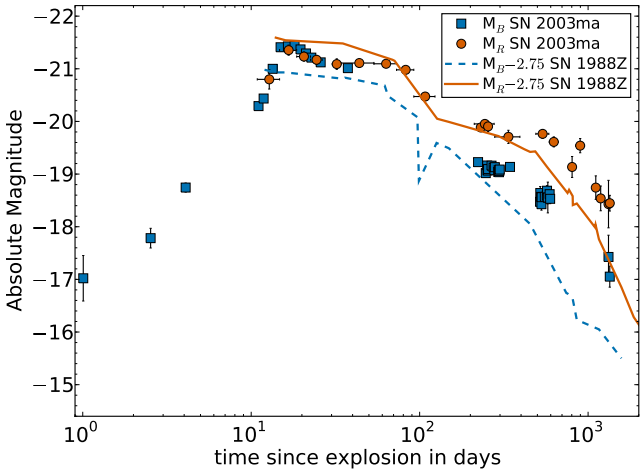

FIG. 12.— Light curve of SN 2003ma in absolute magnitudes in comparison to SN 1988Z in days since explosion, on a log scale. The time axis is in the rest-frame. Offsets have been added to the SN 1988Z absolute magnitudes in order to compare the shape of the light curves. Since the time of explosion is not well constrained for SN 1988Z, we shift the light curves by 12 days to match the bend in the I band light curve of SN 2003ma seen after 100 days.

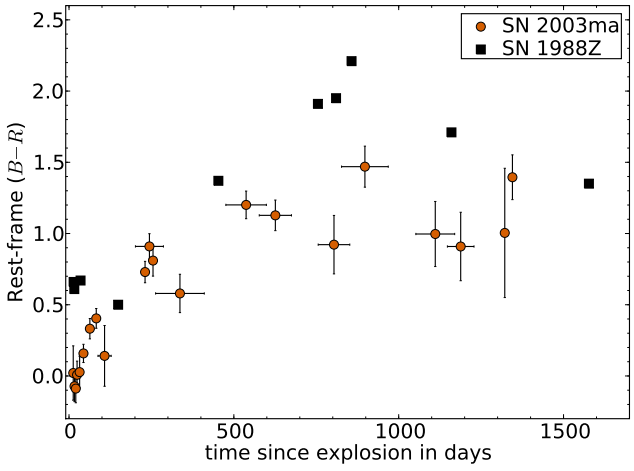

FIG. 13.— Rest-frame $B - R$ colors of SN 2003ma in comparison to SN 1988Z in days since the estimated time of explosion t_0. The time of explosion of SN 1988Z is assumed to be 12 days before discovery. The time axis is in the rest-frame. Both SNe show an increase in $B - R$ color until ∼1000 days, after which the $B - R$ color plateaus.

emitted energy in rest-frame R band is 4.5×10^{50} ergs,

TABLE 5

Observed Passband Y	λ_Y (Å)	A_Y (mag)	Restframe Passband X	K_{XY} (mag)	$L_{\odot,X}$ (10^{32} ergs s^{-1})	$M_{\odot,X}$ (mag)	b_X	E_X (10^{50} ergs)	$E_{\rm bol,X}$ (10^{50} ergs)
$B_{\rm SM}$	4379	1.44	U	0.84	1.89	5.60	20.40		
$VR_{\rm SM}$	5842	1.01	B	−0.63	4.41	5.47	8.72	4.76 (0.12)	41.47 (1.06)
$I_{\rm SM}$	7898	0.66	R	−0.49	6.48	4.46	5.93	4.48 (0.10)	26.57 (0.60)
$I_{\rm OGLE}$	7980	0.65	R	−0.51					
$VR+I$			B+R				3.53	9.24 (0.14)	32.62 (0.49)

NOTE. — Table of K-corrections and bolometric corrections for the solar model. For each of the passbands Y (first column), the effective wavelength λ_Y, extinction A_Y, the passband X that matches best in the restframe, the K-correction K_{XY}, the luminosity $L_{\odot,X}$ of the sun in X, the absolute magnitude $M_{\odot,X}$ of the sun in X, and the bolometric correction b_X are shown in the 2nd-8th column, respectively. The K-correction and bolometric correction are calculated using the solar SED. We combine $I_{\rm SM}$ and $I_{\rm OGLE}$ in all restframe measurements since they match well to the same restframe passband. The 9th column shows the integrated energy E_X in passband X, and the 10th column the integrated bolometric energy $E_{\rm bol,X}$ derived from the passband X photometry. The uncertainties quoted in E_X and $E_{\rm bol,X}$ are the random uncertainties and don't contain any of the systematic errors due to e.g. the interpolation of the lightcurves, K-correction, etc.

TABLE 6

Observed Passband Y	Restframe Passband X	K_{XY} Peak	K_{XY} Plateau 1	K_{XY} Plateau 2	b_X Peak	b_X Plateau 1	b_X Plateau 2	E_X (10^{50} ergs)	$E_{\rm bol,X}$ (10^{50} ergs)
$VR_{\rm SM}$	B	−0.44	−0.54	−0.61	7.62	26.66	27.57	5.04 (0.12)	124.96 (3.40)
$I_{\rm SM}$	R	−0.57	−0.59	−0.74	12.22	3.88	6.15	3.69 (0.08)	22.28 (0.49)
$I_{\rm OGLE}$	R	−0.57	−0.62	−0.80					
$VR+I$	B+R				4.69	3.38	5.03	8.67 (0.13)	40.15 (0.63)

NOTE. — Table of K-corrections and bolometric corrections for the BB15K/88Z model. For each of the passbands Y (first column), the passband X that matches best in the restframe (second column), the K-correction K_{XY}, and the bolometric correction b_X are shown. For both the K-correction and bolometric correction, we use 3 different SED's for the 3 different light curve phases peak, plateau 1, and plateau 2. For the peak, we use a 15,000 K blackbody SED. Since the lightcurve and color evolution of the first and second plateau is similar to that of SN 1988Z, we use a spectrum of SN 1988Z from 04/06/1989 as SED for plateau 1, and an average of SN 1988Z spectra from 04/18/1990, 02/20/91, and 02/04/92 for plateau 2. The K-correction for the peak, plateau 1 and plateau 2 is shown in 3rd, 4th, and 5th column, respectively. The bolometric correction for the peak, plateau 1 and plateau 2 is shown in the 6th, 7th, and 8th column, respectively. We combine $I_{\rm SM}$ and $I_{\rm OGLE}$ in all restframe measurements since they match well to the same restframe passband. The 9th column shows the integrated energy E_X in passband X, and the 10th column the integrated bolometric energy $E_{\rm bol,X}$ derived from the passband X photometry. The uncertainties quoted in E_X and $E_{\rm bol,X}$ are the random uncertainties and don't contain any of the systematic errors due to e.g. the interpolation of the lightcurves, K-correction, etc.

with a similar amount emitted in the rest-frame B band of 4.8×10^{50} ergs. This is more than ten times the energy emitted by SN 1988Z in the B band over roughly the same period of time ($\sim$4.3 year) of $\sim3\times10^{49}$ ergs (Aretxaga et al. 1999). By adding the luminosities in the rest frame B and R together, and integrating over the light curve, we calculate the energy emitted in the combined rest frame B and R to be $E_{B+R}=9.2\times10^{50}$ ergs (black line in lower left panel of Figure 14). When we use the BB15K/88Z model for the K-correction, we get energies in B, R, and $B+R$ of 5.0×10^{50}, 3.7×10^{50}, and 8.7×10^{50} ergs, respectively. These energies differ by only $\lesssim15\%$ from the energies based on the solar model, and we thus estimate that our systematic errors are $\lesssim15\%$.

The bolometric luminosities and hence bolometric energies have a strong dependency on the SED used to calculate the bolometric corrections. The dashed lines in the lower panels of Figure 14 show the bolometric energies derived from the different passbands using the solar and BB15K/88Z model on the left and right, respectively. The bolometric energies based on the solar model agree reasonably well and range between 2.7×10^{51} and 4.1×10^{51} ergs. However, the bolometric energies derived using the BB15K/88Z model significantly differ, e.g., a factor of five between rest frame R (2.2×10^{51} ergs) and B (12.5×10^{51} ergs), even though this model is physically more motivated.

This large difference between the rest frame B and R derived bolometric energy is mainly driven by the bolometric correction based on the SN 1988Z spectra for the two plateau phases. The late-time spectra of SN 1988Z-like SN are dominated by the strong Hα emission line on the one hand, and the blue pseudo-continuum on the other hand. At late phases, this blue continuum is detected in most interacting SNe, e.g., SN 2006jc (Foley et al. 2007), and has been shown by Smith et al. (2009b) to be fluorescence of a forest of emission lines that can only be resolved if the lines are narrow enough, e.g., SN 2005ip. The main difference between the spectral shape of these late-time spectra of SNe IIn is the relative strength of the Hα emission line (rest frame R) compared to the blue pseudo-continuum (rest frame B and bluer). The rest frame $B-R$ color of SN 1988Z is significantly redder than the one of SN 2003ma, indicating that for SN 2003ma the relative strength of the Hα line compared to the UV pseudo-continuum is weaker than for SN 1988Z. Thus using the spectra of SN 1988Z leads to a bolometric over-correction in the rest frame B band and an under-correction in the rest frame R band, which explains the large discrepancy between the two estimated bolometric luminosities. By combining rest frame B and R, this effect gets largely compensated, and the bolometric energy of 4.0×10^{51} ergs is comparable to the bolometric energy using the solar model of

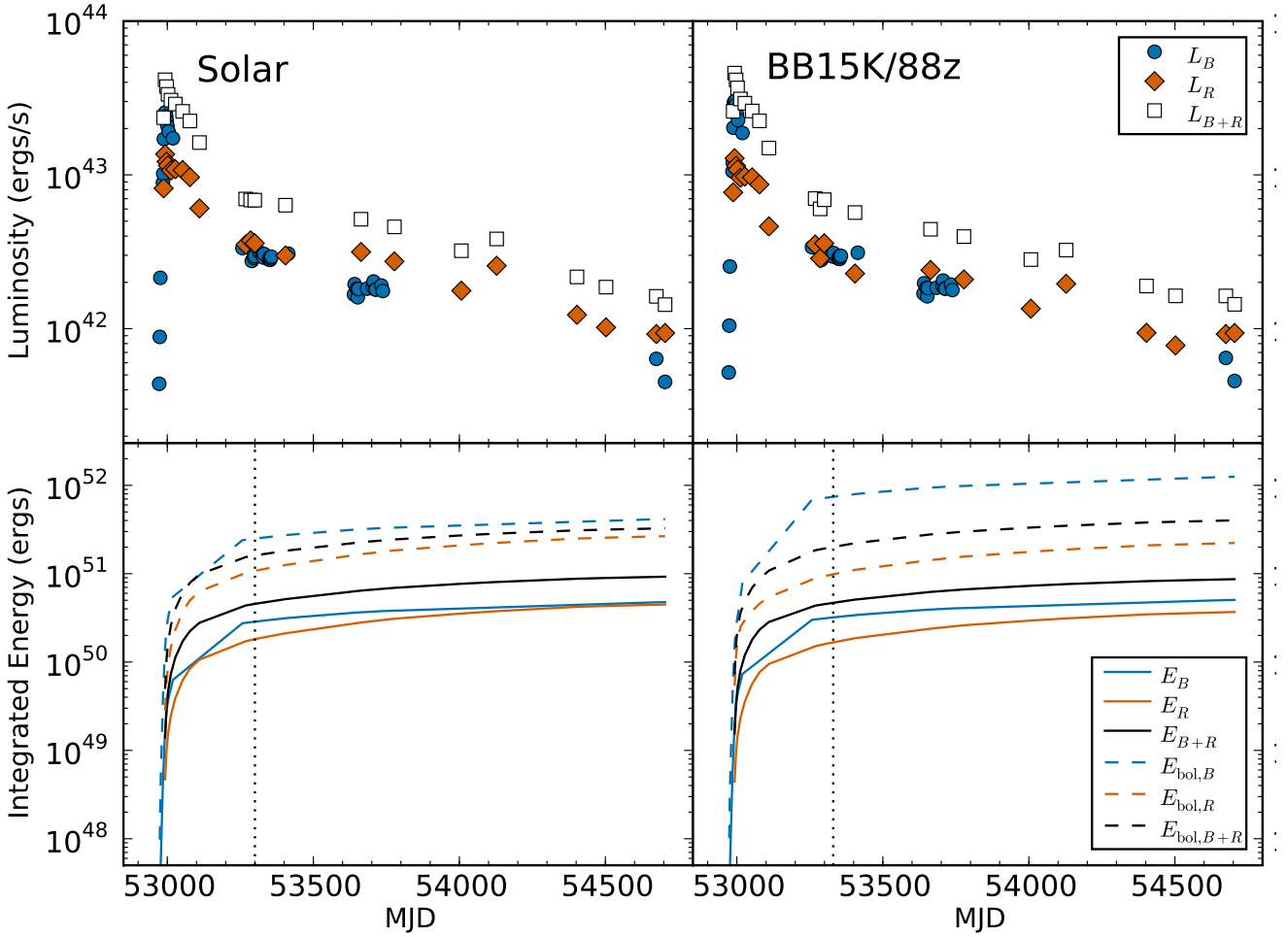

FIG. 14.— Top left: The luminosities in the rest frame B, R and combined $B+R$ passbands using the solar SED for the determination of the K-correction (solar model). Top Right: Same luminosities, but using a 15,000 K blackbody SED for the K-correction during peak, and SEDs from SN 1988Z for the K-corrections during the plateau phase (BB15K/88Z model). Bottom left and right: The integrated emitted energy in the B, R and combined $B+R$ passbands using the solar and BB15K/88Z model, respectively, in solid lines. The dashed lines show the integrated bolometric energy for the two models. See Section 4.5 for a discussion.

3.2×10^{51} ergs. We thus estimate the bolometric radiated energy of SN 2003ma to be $(3.6\pm1)\times10^{51}$ ergs, with the error dominated by the systematic error in the bolometric correction. This is significantly more than the total radiated energy of 2.3 – 2.5 $\times10^{51}$ ergs by SN 2006gy in ∼0.6 years (Smith et al. 2009a), and 1.1×10^{51} ergs for SN 2008es in ∼0.4 years (Miller et al. 2009), and ten times the energy radiated by SN 1988Z over 8.5 years of 3.2×10^{50} ergs (Aretxaga et al. 1999). Analogous to SN 1988Z, the true bolometric luminosity of SN 2003ma is probably a factor of 10 higher if you include emission from the radio to X-rays that is produced from the interaction of the SN shock with the CSM, resulting in a total radiated energy budget of at least 10^{52} ergs.

Even though SN 2003ma is not quite as bright at peak as the most luminous SNe like SNe 2005ap, 2006gy, and 2008es, its total emitted energy is larger since half of the radiated energy is emitted after 350 days due to its very long decline (see the dotted lines in Figure 14 for $E_{\rm bol,B+R}$), at times when the other extremely luminous SNe do not produce any significant radiation. Such a large amount of radiated energy can be achieved if two things coincide: (1) the initial explosion has a large total (combined radiative and kinetic) energy and (2) most of the kinetic energy is converted into radiation by interaction with a CSM.

4.6. *Peak Luminosity*

The peak luminosity of a SN II from thermal energy deposited into the ejecta following shock break out can be estimated to be

$$L_0 = \frac{\beta c}{2\kappa}\frac{E_{\rm SN}R_0}{M} \quad (4)$$

$$= 2.5\times10^{43}\left(\frac{E}{10^{51}{\rm ergs}}\right)\left(\frac{R}{10^{14}{\rm cm}}\right)\left(\frac{M_\odot}{M}\right)\ {\rm ergs\ s^{-1}}, \quad (5)$$

where $E_{\rm SN}$ is the energy of the SN explosion, M is the mass of the ejecta, R_0 is the initial radius of the star, β is a numerical constant related to the radiative diffusion time, and κ is the opacity (Arnett 1996). Thus, the most luminous core-collapse SNe will result from progenitors with large initial radii and low densities. Given the measured total energy emitted in the optical

of $E_{\rm SN} = 4 \times 10^{51}$ ergs, and $L_0 = 5 \times 10^{43}$ ergs s^{-1}, this implies $R_0 = 2 \times 10^{14}\,[M/(10M_\odot)]$ cm, a value approaching the radii of the largest known RSGs (Levesque et al. 2005). If the progenitor were an Eta Carinae-type massive star with $M \approx 100M_\odot$, this would require a radius ten times larger, which is difficult to reconcile with stellar radii predicted by stellar evolutionary models.

If the peak of the light curve is powered solely by radioactive decay, we expect

$$M_{\rm Ni}/M_\odot = \frac{L}{1.42 \times 10^{43}\ {\rm ergs\ s^{-1}}} e^{(t/111{\rm days})}. \quad (6)$$

For SN 2003ma, which had $L_{\rm peak} = 5 \times 10^{43}$ ergs s^{-1} at $t = 8.5$ days after explosion in the SN rest-frame, the initial ^{56}Ni mass is 4 $M_\odot$, which is one to two orders of magnitude larger than typically produced in SNe IIP (Hamuy 2003). Although this amount of ^{56}Ni could be produced in a pair-instability explosion (Scannapieco et al. 2005), the slow rise to maximum and constant slope of decay after maximum in such models are incompatible with the light curve of SN 2003ma.

4.7. *Kinetic Energy*

Measuring the kinetic energy from a SN typically requires an ejecta mass and a velocity for the ejecta. For SN 2003ma we were unable to measure the velocity of the ejecta from any of our spectra. However, we can estimate the energy converted from shock energy to kinetic energy by examining the velocity of the post-shock material. If we assume that the pre-shock circumstellar material has a coherent velocity, $v_{\rm w}$ and a mass, m, it has a kinetic energy,

$$E_0 = \frac{1}{2} m v_{\rm w}^2. \quad (7)$$

If we assume that the post-shock material has a one-dimensional RMS velocity, $v_{\rm ps}$, then the post-shock kinetic energy of the circumstellar material is

$$E_{\rm ps} = \frac{3}{2} m v_{\rm ps}^2, \quad (8)$$

and the shock deposited an energy,

$$\Delta E = \frac{1}{2} m (3v_{\rm ps}^2 - v_{\rm w}^2). \quad (9)$$

If we assume that the pre-shock circumstellar material has a constant density, ρ, and that the shock traveled at a velocity of $v_{\rm s}$ with no appreciable deceleration, then

$$m = \frac{4}{3} \pi \rho (v_{\rm s} t)^3 \quad (10)$$

is the mass of circumstellar material swept up by the shock in a time t after explosion.

Combining Equations 9 and 10 and assuming that $v_{\rm ps} \gg v_{\rm w}$, we find

$$\Delta E = 2\pi \rho v_{\rm ps}^2 v_{\rm s}^3 t^3. \quad (11)$$

If we have a constant conversion of kinetic energy to luminosity, then $L = \eta \Delta E/t$, where η is the efficiency factor. The density can then be written as

$$\rho = 5.6 \times 10^{-20} \frac{1}{\eta} \frac{L}{10^{42}\ {\rm ergs\ s^{-1}}} \left(\frac{v_{\rm ps}}{6000\ {\rm km\ s^{-1}}} \right)^{-2} \times \left(\frac{v_{\rm s}}{20,000\ {\rm km\ s^{-1}}} \right)^{-3} \left(\frac{t}{\rm year} \right)^{-2}\ {\rm g\ cm^{-3}}. \quad (12)$$

¿From Equations 10 and 12, we have the total swept-up mass,

$$m = 0.03 \frac{1}{\eta} \frac{L}{10^{42}\ {\rm ergs\ s^{-1}}} \left(\frac{v_{\rm ps}}{6000\ {\rm km\ s^{-1}}} \right)^{-2} \left(\frac{t}{\rm year} \right) M_\odot, \quad (13)$$

which is independent of any assumed ejecta velocity. At the time of the last spectrum, when $L = 5 \times 10^{42}$ ergs s^{-1}, $v_{\rm ps} = 6000$ km s^{-1}, and $t = 3.9$ years, SN 2003ma had swept up 0.6 $M_\odot$ of circumstellar material and had at least 6.4×10^{50} ergs of kinetic energy if $\eta = 1$. These values are lower limits since if $\eta < 1$, the swept-up mass and kinetic energy increases.

4.8. *Dust*

The *Spitzer* photometry in IRAC bands 1 – 4 and MIPS band 1 (see Table 2) is shown in Figure 15 with respect to the rest wavelengths (2.8, 3.5, 4.5, 6.2, and 18.5 μm, respectively) corresponding to the observed wavelengths of 3.6, 4.5, 5.8, 8.0, and 24 μm, respectively. There is a significant difference between the first epoch (2005 July 15 – 26; ∼580 days after maximum) and the second epoch (2005 October 26 – November 2; ∼675 days after maximum) at restframe 3.5, 4.5, and 6.2 μm: the fluxes at 3.5 and 6.2 μm increase by 4σ and 10σ, respectively, whereas the 4.5 μm flux decreases by 4σ. Note that we use the relative flux error for the comparison of fluxes at different epochs, but the same filter (4th column in Table 2), as we have discussed in Section 2.2. For all comparisons of fluxes from different bands, we use the total errors (6th column in Table 2), which includes the wavelength dependent error introduced by the crowdedness of the field.

Such a significant change in flux over such a short time span makes it highly likely that at least some of the measured infrared flux is caused by the SN. Note, however, that the direction of these differences across the bands is not in the same direction in neighboring bands, and therefore SN 2003ma would not have been considered a variable candidate according to the criteria used by Vijh et al. (2009) for the SAGE-LMC variables list. The observed 24 μm flux is essentially unchanged and is either an IR echo as observed for other SNe (e.g., SN 2002hh, Barlow et al. 2005; Meikle et al. 2006; SN 2004et, Kotak et al. 2009) or from other sources in the host galaxy.

The changes in flux cannot be explained by a simple change in temperature and/or flux of a blackbody, but rather requires emission bands of molecules or dust. The first detection of carbon monoxide (CO) in a SN in the fundamental (4.6 μm) and first overtone (2.3 μm) bands was in the spectra of SN 1987A (Catchpole et al. 1987; McGregor et al. 1987; Oliva et al. 1987; Spyromilio et al. 1988). In addition to CO, silicon monoxide (SiO) emission bands were detected in SN 1987A at 7.9 and 8.5 μm (Roche et al.

1991; Meikle et al. 1993; Liu & Dalgarno 1994). Subsequently, MIR CO lines were detected in SNe 1995ad (Spyromilio & Leibundgut 1996), 1998S (Gerardy et al. 2000; Fassia et al. 2001), 1998dl (Spyromilio et al. 2001), 1999em (Spyromilio et al. 2001), 2000ew (Gerardy et al. 2002b) and 2004et (Kotak et al. 2009), which also showed SiO lines. The wavelengths of the CO and SiO emission bands are indicated in Figure 15. The match between the CO and SiO lines with the observed flux changes is poor, except for possible contribution of the CO fundamental band at 4.6 μm. However, we note that for both SNe 1987A and 2004et the CO and SiO bands appeared ∼100 days after maximum and disappeared by ∼500 days, significantly earlier than the increase seen in the second epoch for SN 2003ma.

Another possible explanation is that the strong and variable emission detected in the 8 μm IRAC band is from the 6.2 μm emission feature of polycyclic aromatic hydrocarbon (PAH) nanoparticles. Such emission is routinely detected in the Milky Way and other galaxies (e.g., Genzel & Cesarsky 2000; Vogler et al. 2005; Irwin & Madden 2006; Draine & Li 2007; Smith et al. 2007a).

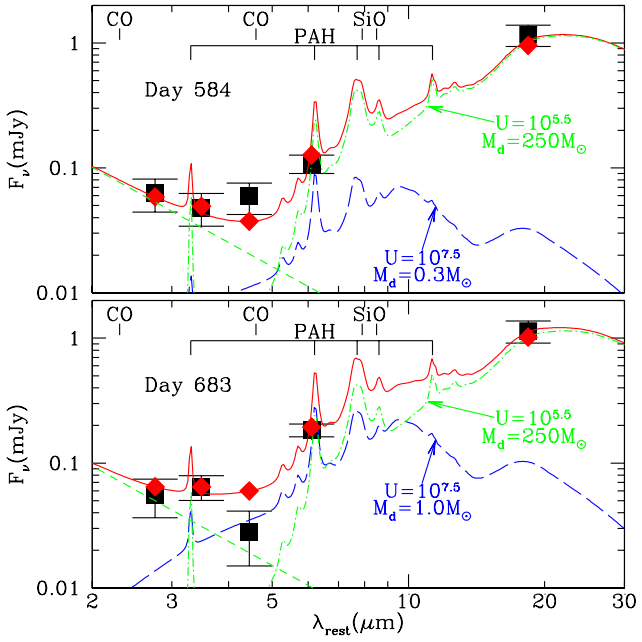

FIG. 15.— Spitzer IRAC (3.6, 4.5, 6.0, and 8.0 μm) and MIPS (24 μm) photometry versus rest wavelength, for 584 and 683 days after maximum. The solid curves show models which include hot dust, warm dust (see text), and a stellar component with a Rayleigh-Jeans spectrum. Filled diamonds are the model convolved with the IRAC and MIPs response functions. The photometry is consistent with the observed emission consisting of steady emission from warm dust in the galaxy, plus a time-variable IR echo produced by hot dust.

Here we present a dust model that could explain the observed IR emission. First, we assume that the bulk of the emission observed at 3.6 μm (rest frame 2.3 μm) is stellar continuum and we extrapolate this to longer wavelengths assuming a Rayleigh-Jeans spectrum (short-dashed line in Figure 15). To this we add emission from a mixture of PAHs, graphite, and silicate dust, from the dust models of Draine & Li (2007). For SN 2003ma we assume the radiation field heating the dust to have the spectrum of a 15,000 K blackbody, and have solved for the temperature distribution functions for different grain sizes and compositions, and different radiation intensities. The emission model has two components: steady emission from the "warm" dust in the galaxy, plus a time-varying IR echo from "hot" dust heated by radiation from the SN.

To reproduce the 24 μm photometry, the warm dust must be hot enough for the silicate 18 μm feature to emit strongly. This is accomplished by a radiation field with $U \approx 10^{5.5}$ (U is the dust heating rate relative to heating by the starlight background in the solar neighborhood). This dust component is assumed to have the same ionization fraction as a function of grain size as assumed by DL07 for the Galaxy, and which has been found to work well for the IR-submm emission from, e.g., the galaxies in the SINGS sample (Draine et al. 2007). The PAH abundance in the warm dust component must be low, $q_{\rm PAH} \approx 0.5\%$, in order to not overproduce the observed flux in IRAC bands 2 and 4. This component has a dust mass of $\sim 250 M_\odot$; for a normal dust-to-gas ratio, this corresponds to a hydrogen mass of $\sim 2.5 \times 10^4 M_\odot$. This is a plausible amount of gas for hot photodissociation regions in a starburst galaxy. The spectrum of this emission is shown in Figure 15. The total IR luminosity of this dust component is $\sim 1.1 \times 10^{10} L_\odot$. There is presumably additional emission from a much larger mass of cool dust in the galaxy, but we lack longer wavelength observations to constrain this component.

The dust producing the IR echo is assumed to be very strongly heated, with $U \approx 10^{7.5}$. The IR echo dust mass is $\sim 0.3 M_\odot$ on day 584, and $\sim 1 M_\odot$ on day 683. The total IR luminosity of this component on day 683 is $\sim 4 \times 10^9 L_\odot$, requiring that the IR echo dust be absorbing a substantial fraction of the SN light. This dust is assumed to have a PAH abundance $q_{\rm PAH} = 4.7\%$, similar to the PAH abundance in many solar-metallicity star-forming galaxies. The PAHs are assumed to be ionized by the radiation from the SN; the PAH neutral fraction in this component is assumed to be negligible (the absence of neutral PAHs lowers the ratio of 3.3 μm emission relative to 7.7 and 8.6 μm emission, which is needed in order to not overproduce the emission into IRAC band 2). The intense radiation heats the large grains to $T \approx 300$ K; the contribution of the broad 9.7 μm silicate feature is apparent in this component of the model spectrum. Even in this intense radiation field, the emission in the 3.3 and 6.2 μm PAH features continues to be due primarily to single-photon heating.

This two component model, with the mass of the hot dust increasing by a factor ∼3 between days 584 and 683, reproduces most of the IR photometry. There is admittedly a discrepancy with the observed flux density in IRAC band 3 ($\lambda_{\rm rest} = 4.5$ μm): the observed flux decreases by a factor ∼3 between days 584 and 683, and our model does not reproduce this. Perhaps CO 1-0 4.6 μm emission (not included in our model) contributes to the high flux measured on day 584.

The dust heating parameter $U = 10^{7.5}$ corresponds to an energy density $u(h\nu < 13.6{\rm eV}) = 4 \times 10^{-5}$ erg cm^{-3}. The distance of the dust from the SN is not known, but it is reasonable to assume a distance ∼600 light-days

(0.50 pc). For this distance, the SN luminosity required to produce $U = 10^{7.5}$ is $\sim 1.4 \times 10^{10} L_{\odot}$ – consistent with the photometry in Figure 14.

A sphere of radius 0.5 pc with density $n_{\rm H} = 8 \times 10^3$ cm^{-3} contains $M_d \approx 1 M_{\odot}$ of dust (assuming $M_d/M_{\rm H} \approx 0.01$). Densities $n_{\rm H} \gtrsim 10^4$ cm^{-3} would be expected for cool gas in the high-pressure environment of a starburst galaxy. The IR echo requires $\sim 1 M_{\odot}$ of dust at a distance $\sim$0.5 pc from the SN to produce the IR echo. This dust could be located in an interstellar cloud, or possibly in a swept-up shell of interstellar matter surrounding a stellar-wind bubble.

To summarize: (1) PAH emission features can explain the increase in the observed 4.5 and 8 μm flux densities; (2) the required dust mass of $M_d \approx 1 M_{\odot}$ should be $\sim$0.5 pc from the SN, which is reasonable; (3) the intensity of the SN radiation at this distance is consistent with what is required to heat the dust to reproduce the observed emission. We conclude that the observed IR photometry of LMC 902 is consistent with an IR echo produced by normal interstellar dust at a distance $\sim$0.5 pc from the SN. We note, however, that the data does not sufficiently constrain the model to make it unique, and other explanations are possible.

5. CONCLUSIONS

This paper presents photometry and spectroscopy of SN 2003ma, an exceptional SN IIn at a redshift of $z = 0.289$ behind the Large Magellanic Cloud.

SN 2003ma has an I-band light curve with two long plateaus, and strong emission in the V and I bands for $\sim$1000 days, reminiscent of the long-lived emission seen in interacting SNe IIn like the prototype of the class, SN 1988Z. However, in contrast to all other SNe IIn with long-lived plateaus, SN 2003ma also has an exceptionally bright peak luminosity of $M_R = -21.5$ mag, placing it in the class of extremely luminous core-collapse SNe, such as SNe 2005ap, 2006gy, 2008es, and 2008fz. The combination of high peak luminosity and long-lasting plateau makes SN 2003ma more luminous than any other SN at 80 days past maximum brightness. Consequently, half of the radiated energy is emitted after 350 days past maximum light, while other extremely luminous SNe produce no significant radiation at such late times.

The derived bolometric luminosity, and hence bolometric energy, has a strong dependency on the SED used to calculate the bolometric corrections. In order to estimate the systematic bias of the assumed SED, we use different SEDs to calculate the bolometric corrections. Integrating the bolometric light curve, we find that a total bolometric output of $\sim 4 \times 10^{51}$ ergs was emitted over 4.7 years – more than twice the total radiated energy of SNe 2006gy or 2008es, and ten times the energy radiated by SN 1988Z, making SN 2003ma the most energetic SN ever observed with respect to its radiative output. This value alone is within an order of magnitude of the maximum energy that a core-collapse explosion can produce outside of the neutrino channel.

The nearly flat late-time light curve over the long timespan of several years in combination with the persistent single-peaked intermediate-width Hα emission line are best explained by the conversion of the kinetic energy of the explosion into radiation by strong interaction of the SN with a dense circumstellar material. SN 2003ma is distinct from proto-typical SNe IIn in that the intermediate width line is unusually broad, and it does not have a broad component. If SN 2003ma has narrow emission lines cannot be answered conclusively since it is difficult to separate the narrow emission lines from the SN, if they exist, from the narrow emission lines of the starbursting host.

The fast velocity measured for the intermediate-width Hα component ($\sim$6000 km s^{-1}) also points towards an extremely energetic explosion ($> 10^{52}$ ergs) which imparts a faster blast-wave speed to the postshock material and a higher luminosity from the interaction than is observed in typical SNe IIn such as SN 1988Z. The large amount of radiated energy can only be achieved if the initial explosion has a large total radiative and kinetic energy and most of its kinetic energy is converted into radiation by interaction with a CSM. A conventional core-collapse SN explosion can produce at most a few times 10^{52} ergs of energy that can couple to baryonic matter. The measured kinetic energy of SN 2003ma is comparable to this limit (and similar to GRB-associated SNe), and therefore SN 2003ma may have been produced by an alternative explosion mechanism such as the pair-instability SN.

The *Spitzer* IR photometry shows significant variations in the IR from 584 days to 683 days after maximum in restframe 3.5, 4.5, and 6.2 μm. Such a significant change in flux over such a short time span makes it highly likely that at least some of the measured infrared flux is caused by the SN. The changes in flux cannot be explained by a simple change in temperature and/or flux of a blackbody, but rather requires emission bands of molecules or dust. We find that the observed increase in the IR flux density at 4.5 and 8.0 μm is consistent with an IR echo of the SN produced by normal interstellar dust at a distance $\sim$0.5 pc from the SN in combination with PAH emission features.

By any measure, SN 2003ma is a remarkable object. Its discovery and extensive lightcurve coverage were made possible by long-duration microlensing surveys. Its prompt identification and initial spectrocopy reveal the power of well-implemented reduction pipelines and planned, timely coordination of large telescope facilities. The inclusion of satellite data provided important constraints of the environment of this object. Ground-based facilities devoted entirely to deep, time-domain discovery such as the Large Synoptic Survey Telescope and PanSTARRS are almost certain to reveal many more such objects and lead us towards even greater understanding of the progenitors required to produce extremely luminous core-collapse supernovae like SN 2003ma and illuminate the full range of observational characteristics for what, for now, remains a small and elusive set of truly cataclysmic events.

APPENDIX

CLASSIFICATION OF SN 2003MA

In this section we summarize why we classify SN 2003ma as a SN and not one of these other options.

Event in Milky Way or LMC

From Figure 2, we see that SN 2003ma is 0.064 ± 0.012 arcsec from a resolved source in our template images. In 2008, SN 2003ma was much fainter than this source; therefore, our 2008 spectrum is dominated by this source, a starburst galaxy at $z = 0.289$. If the event is in the LMC or Milky Way, then it must be either a transient or variable source with a quiescent brightness $\gtrsim 5$ mag fainter than at peak. This excludes most flaring variable stars such as M dwarfs and Ae/Be stars since the amplitude of their flares are generally small compared to the total flux. Additionally, we would not expect a prolonged, > 5 year decline from peak.

Another candidate is a nova, which could flare by > 5 mag. However, our spectra from 2003 does not show any emission lines at or near zero redshift, which we would expect since the event is 0.5 magnitude brighter than the source at that time and therefore should dominate the spectrum. Furthermore, the light curve is unlike any nova yet observed.

Considering all this, it is unlikely that SN 2003ma occurred in either the LMC or Milky Way.

Supermassive Black Hole Event

AGN are often variable at various time-scales. Here we discuss if it is likely that SN 2003ma is an AGN.

- If SN 2003ma originates from a black hole in the supposed host galaxy then the supermassive black hole is offset by 500 pc from the center of the galaxy.

- We calculate the weighted average of 42 SuperMACHO *VR* difference image fluxes before the event (MJD $\leq$ 52965) spanning 2 years, and find that it is within 1σ of zero, with a reduced $\chi^2 = 1.2$. None of the 42 detections deviates from zero by more than 3σ, and typical 3σ lower limits on variability are 24.2 magnitudes. If we split up these 42 detections into three blocks 52224 $\leq$ MJD $\leq$ 52291, 52547 $\leq$ MJD $\leq$ 52643, and 52932 $\leq$ MJD $\leq$ 52965, we find again that the average fluxes are consistent with zero with reduced χ^2 of 1.01, 0.96, and 1.73, respectively. Therefore the pre-event variability in *VR* is fainter than 24.2 magnitude during this 2-year time period.

  We perform a similar analysis with the *I* band light curve and find that the pre-event OGLE-II (MJD $<$ 52091) and OGLE-III (52091 $\leq$ MJD $<$ 52965) data is consistent with being constant with a reduced χ^2 of 1.65 and 1.51, respectively. We 3σ-clipped 4% of the data. When we bin the data (see Section 2.1 and bottom panel in Figure 3), we find that all average fluxes are within 3σ of zero, with reduced χ^2 ranging from 0.67 to 1.91.

- Another test for the presence of AGN activity in the host galaxy are the ratios of the narrow emission lines, which are measured for all spectra and presented in Table 4. The [O III]/Hβ and [N II]/Hα, and [S II]/Hα ratios in the standard diagnostic line ratios (Baldwin et al. 1981; Veilleux & Osterbrock 1987) classify the host galaxy as a star-forming galaxy. Although the emission lines may have a contribution from the transient object, in the post-peak spectra from $2004 - 2008$ the [O III]/Hβ, [N II]/Hα, and [S II]/Hα ratios are constant within the errors, which implies that at late times the narrow-line emission is dominated by the host galaxy.

- We consider the rare case in which an otherwise dormant supermassive black hole tidally disrupts a star, and emits a flare of radiation from the accretion of the stellar debris. This could explain that the event itself is about 0.5 magnitude brighter than the host and shows no variability pre-event. These events are typically bright in the X-rays (Komossa 2002; Esquej et al. 2007) and UV (Gezari et al. 2006, 2008, 2009b), however several candidates have emerged that have also been detected at optical wavelengths (Gezari et al. 2008, 2009b). The strong evolution of the foreground extinction-corrected colors of SN 2003ma from $V - I \approx 0$ at peak to $V - I > 1$ for times later than 1 year after the peak (see Section 4.3), however, are inconsistent with the steady blue colors expected for the blackbody spectral energy distributions and effective temperatures associated with tidal disruption events ($T_{\rm BB} > 1 \times 10^4$ K; Gezari et al. 2009b).

The narrow-line ratios, listed in Table 4, are all consistent with a star-forming galaxy. This, in combination with the lack of variability in the densely sampled SuperMACHO and OGLE difference imaging data over a baseline of 7 years before the SN, place strong constraints on the presence of an AGN in the host galaxy.

Supernova

Since SN 2003ma is unlikely to be caused by a supermassive black hole or Galactic or LMC variable, the remaining likely transient phenomenon is that of a SN. Its blue continuum in 2003 (see Figures 5 and 10) and $\sim$6000 km s^{-1} FWHM emission lines consistent with Hα in 2004 and 2008 are reminiscent of a SN of type IIn (Schlegel 1990). This identification is also consistent with the host galaxy being a star-forming galaxy. In Sections 3.1 and 3.2, we compare the spectroscopy and photometry of SN 2003ma to other SNe from the literature, and we find that the most consistent explanation for this event is that it is a SN IIn.

We thank the referee for many insightful comments that helped to improve this paper. The SuperMACHO survey was undertaken under the auspices of the NOAO Survey Program. We are very grateful for the support provided to the Survey program from the NOAO and the National Science Foundation. We are particularly indebted to the scientists and staff at the Cerro Tololo Inter-American Observatory for their assistance in helping us carry out the survey. SuperMACHO is supported by the STScI grant GO-10583. AR thanks the NOAO Goldberg Fellowship Program for its support. AG's, KHC's, MEH's, and SN's work was performed under the auspices of the U.S. Department of Energy by Lawrence Livermore National Laboratory under Contract DE-AC52-07NA27344. C. Stubbs thanks the the McDonnell Foundation for its support through a Centennial Fellowship. C. Stubbs, AG, and AR are also grateful for support from Harvard University. AC and GP acknowledges the support of grant P06-045-F ICM-MIDEPLAN. DM, AC, and GP are supported by grants FONDAP CFA 15010003 and Basal CATA 0609. LM is supported by grant (CPDR061795/06) from Padova University. DLW acknowledges financial support in the form of a Discovery Grant from the Natural Sciences and Engineering Research Council of Canada (NSERC). LW acknowledges support by the EC FR7 grant PERG04-GA-2008-234784. Based on observations obtained as part of the GS-2003B-Q-12 science program at the Gemini Observatory, which is operated by the Association of Universities for Research in Astronomy, Inc., under a cooperative agreement with the US National Science Foundation on behalf of the Gemini partnership: the NSF (United States), the Science and Technology Facilities Council (United Kingdom), the National Research Council (Canada), CONICYT (Chile), the Australian Research Council (Australia), Ministério da Ciência e Tecnologia (Brazil) and Ministerio de Ciencia, Tecnología e Innovación Productiva (Argentina). The OGLE project is partially supported by the Polish MNiSW grant N20303032/4275.

REFERENCES

Agnoletto, I., et al. 2009, ApJ, 691, 1348
Allington-Smith, J., et al. 1994, PASP, 106, 983
Aretxaga, I., Benetti, S., Terlevich, R. J., Fabian, A. C., Cappellaro, E., Turatto, M., & della Valle, M. 1999, MNRAS, 309, 343
Arnett, D. 1996, Supernovae and nucleosynthesis. an investigation of the history of matter, from the Big Bang to the present (Princeton University Press)
Baldwin, A., Phillips, M. M., & Terlevich, R. 1981, PASP, 93, 817
Barbon, R., Benetti, S., Rosino, L., Cappellaro, E., & Turatto, M. 1990, A&A, 237, 79
Barkat, Z., Rakavy, G., & Sack, N. 1967, Physical Review Letters, 18, 379
Barlow, M. J., et al. 2005, ApJ, 627, L113
Blondin, S., Prieto, J. L., Patat, F., Challis, P., Hicken, M., Kirshner, R. P., Matheson, T., & Modjaz, M. 2009, ApJ, 693, 207
Bond, J. R., Arnett, W. D., & Carr, B. J. 1984, ApJ, 280, 825
Cardelli, J. A., Clayton, G. C., & Mathis, J. S. 1989, ApJ, 345, 245
Catchpole, R., et al. 1987, IAU Circ., 4457, 1
Chevalier, R. A., & Fransson, C. 1994, ApJ, 420, 268
Colina, L., Bohlin, R. C., & Castelli, F. 1996, AJ, 112, 307
Dessart, L., et al. 2008, ApJ, 675, 644
Dessart, L., & Hillier, D. J. 2006, A&A, 447, 691
Dessart, L., Hillier, D. J., Gezari, S., Basa, S., & Matheson, T. 2009, MNRAS, 394, 21
Di Carlo, E., et al. 2002, ApJ, 573, 144
Draine, B. T., et al. 2007, ApJ, 663, 866
Draine, B. T., & Li, A. 2007, ApJ, 657, 810
Drake, A. J., et al. 2010, ApJ, 718, L127
Elmhamdi, A., et al. 2003, MNRAS, 338, 939
Esquej, P., Saxton, R. D., Freyberg, M. J., Read, A. M., Altieri, B., Sanchez-Portal, M., & Hasinger, G. 2007, A&A, 462, L49
Fassia, A., et al. 2001, MNRAS, 325, 907
Filippenko, A. V. 1982, PASP, 94, 715
Foley, R. J., et al. 2009, AJ, 138, 376
——. 2003, PASP, 115, 1220
Foley, R. J., Smith, N., Ganeshalingam, M., Li, W., Chornock, R., & Filippenko, A. V. 2007, ApJ, 657, L105
Fox, O., et al. 2009, ApJ, 691, 650
Fransson, C., et al. 2002, ApJ, 572, 350
Gal-Yam, A., et al. 2009, Nature, 462, 624
Garg, A., et al. 2007, AJ, 133, 403
Genzel, R., & Cesarsky, C. J. 2000, ARA&A, 38, 761
Gerardy, C. L., Fesen, R. A., Höflich, P., & Wheeler, J. C. 2000, AJ, 119, 2968
Gerardy, C. L., et al. 2002a, ApJ, 575, 1007
Gerardy, C. L., Fesen, R. A., Nomoto, K., Maeda, K., Hoflich, P., & Wheeler, J. C. 2002b, PASJ, 54, 905
Gezari, S., et al. 2008, ApJ, 676, 944
——. 2009a, ApJ, 690, 1313
——. 2009b, ApJ, 698, 1367
——. 2006, ApJ, 653, L25
Hamuy, M. 2003, ApJ, 582, 905
Hook, I. M., Jørgensen, I., Allington-Smith, J. R., Davies, R. L., Metcalfe, N., Murowinski, R. G., & Crampton, D. 2004, PASP, 116, 425
Horne, K. 1986, PASP, 98, 609
Irwin, J. A., & Madden, S. C. 2006, A&A, 445, 123
Iwamoto, K., et al. 1998, Nature, 395, 672
Kelson, D. D. 2003, PASP, 115, 688
Kennicutt, Jr., R. C. 1998, ARA&A, 36, 189
Komossa, S. 2002, in Lighthouses of the Universe: The Most Luminous Celestial Objects and Their Use for Cosmology, ed. M. Gilfanov, R. Sunyeav, & E. Churazov, 436–+
Kotak, R., et al. 2009, ApJ, 704, 306
Kozasa, T., Hasegawa, H., & Nomoto, K. 1989, ApJ, 344, 325
Kozłowski, S., et al. 2010, ApJ, 722, 1624
Lejeune, T., Cuisinier, F., & Buser, R. 1997, A&AS, 125, 229
Leonard, D. C., Filippenko, A. V., Barth, A. J., & Matheson, T. 2000, ApJ, 536, 239
Leonard, D. C., et al. 2002, PASP, 114, 35
Levesque, E. M., Massey, P., Olsen, K. A. G., Plez, B., Josselin, E., Maeder, A., & Meynet, G. 2005, ApJ, 628, 973
Li, W., et al. 2010, ArXiv e-prints, 1006.4612
Liu, W., & Dalgarno, A. 1994, ApJ, 428, 769
Marshall, J. L., et al. 2008, in Society of Photo-Optical Instrumentation Engineers (SPIE) Conference Series, Vol. 7014, Society of Photo-Optical Instrumentation Engineers (SPIE) Conference Series
McGregor, P. J., Hyland, A. R., & Beresford, A. C. 1987, IAU Circ., 4468, 2
Meikle, W. P. S., et al. 2006, ApJ, 649, 332
Meikle, W. P. S., Spyromilio, J., Allen, D. A., Varani, G.-F., & Cumming, R. J. 1993, MNRAS, 261, 535
Meixner, M., et al. 2006, AJ, 132, 2268
Miknaitis, G., et al. 2007, ApJ, 666
Miller, A. A., et al. 2009, ApJ, 690, 1303
Moseley, S. H., Dwek, E., Glaccum, W., Graham, J. R., & Loewenstein, R. F. 1989, Nature, 340, 697
Ofek, E. O., et al. 2007, ApJ, 659, L13
Oliva, E., Moorwood, A. F. M., & Danziger, I. J. 1987, IAU Circ., 4484, 1
Pastorello, A., et al. 2010, ArXiv e-prints, 1008.2674
Quimby, R. M., Aldering, G., Wheeler, J. C., Höflich, P., Akerlof, C. W., & Rykoff, E. S. 2007, ApJ, 668, L99
Quimby, R. M., et al. 2009, Nature, submitted (arXiv:0910.0059)
Rest, A., et al. 2005, ApJ, 634, 1103
Rho, J., et al. 2008, ApJ, 673, 271
Riess, A. G., et al. 2005, ApJ, 627, 579

Roche, P. F., Aitken, D. K., & Smith, C. H. 1991, MNRAS, 252, 39P
Scannapieco, E., Madau, P., Woosley, S., Heger, A., & Ferrara, A. 2005, ApJ, 633, 1031
Schechter, P. L., Mateo, M., & Saha, A. 1993, PASP, 105, 1342
Schlegel, D. J., Finkbeiner, D. P., & Davis, M. 1998, ApJ, 500, 525
Schlegel, E. M. 1990, MNRAS, 244, 269
Smith, J. D. T., et al. 2007a, ApJ, 656, 770
Smith, N., Chornock, R., Li, W., Ganeshalingam, M., Silverman, J. M., Foley, R. J., Filippenko, A. V., & Barth, A. J. 2008a, ApJ, 686, 467
Smith, N., Chornock, R., Silverman, J. M., Filippenko, A. V., & Foley, R. J. 2009a, ApJ, submitted (arXiv:0906.2200)
Smith, N., Foley, R. J., & Filippenko, A. V. 2008b, ApJ, 680, 568
Smith, N., et al. 2007b, ApJ, 666, 1116
——. 2009b, ApJ, 695, 1334
Sollerman, J., Cumming, R. J., & Lundqvist, P. 1998, ApJ, 493, 933
Spyromilio, J., & Leibundgut, B. 1996, MNRAS, 283, L89
Spyromilio, J., Leibundgut, B., & Gilmozzi, R. 2001, A&A, 376, 188
Spyromilio, J., Meikle, W. P. S., Learner, R. C. M., & Allen, D. A. 1988, Nature, 334, 327
Stetson, P. B. 1987, PASP, 99, 191
Sugerman, B. E. K., et al. 2006, Science, 313, 196
Trundle, C., et al. 2009, A&A, 504, 945
Turatto, M., Cappellaro, E., Danziger, I. J., Benetti, S., Gouiffes, C., & della Valle, M. 1993, MNRAS, 262, 128
Udalski, A. 2003, Acta Astronomica, 53, 291
Udalski, A., Kubiak, M., & Szymanski, M. 1997, Acta Astronomica, 47, 319
Udalski, A., et al. 2008, Acta Astronomica, 58, 89
Veilleux, S., & Osterbrock, D. E. 1987, ApJS, 63, 295
Vijh, U. P., et al. 2009, AJ, 137, 3139
Vogler, A., Madden, S. C., Beck, R., Lundgren, A. A., Sauvage, M., Vigroux, L., & Ehle, M. 2005, A&A, 441, 491
Wade, R. A., & Horne, K. 1988, ApJ, 324, 411
Woosley, S., & Janka, T. 2005, Nature Physics, 1, 147
Woosley, S. E. 1993, ApJ, 405, 273
Woosley, S. E., Blinnikov, S., & Heger, A. 2007, Nature, 450, 390
Wozniak, P. R. 2000, Acta Astronomica, 50, 421

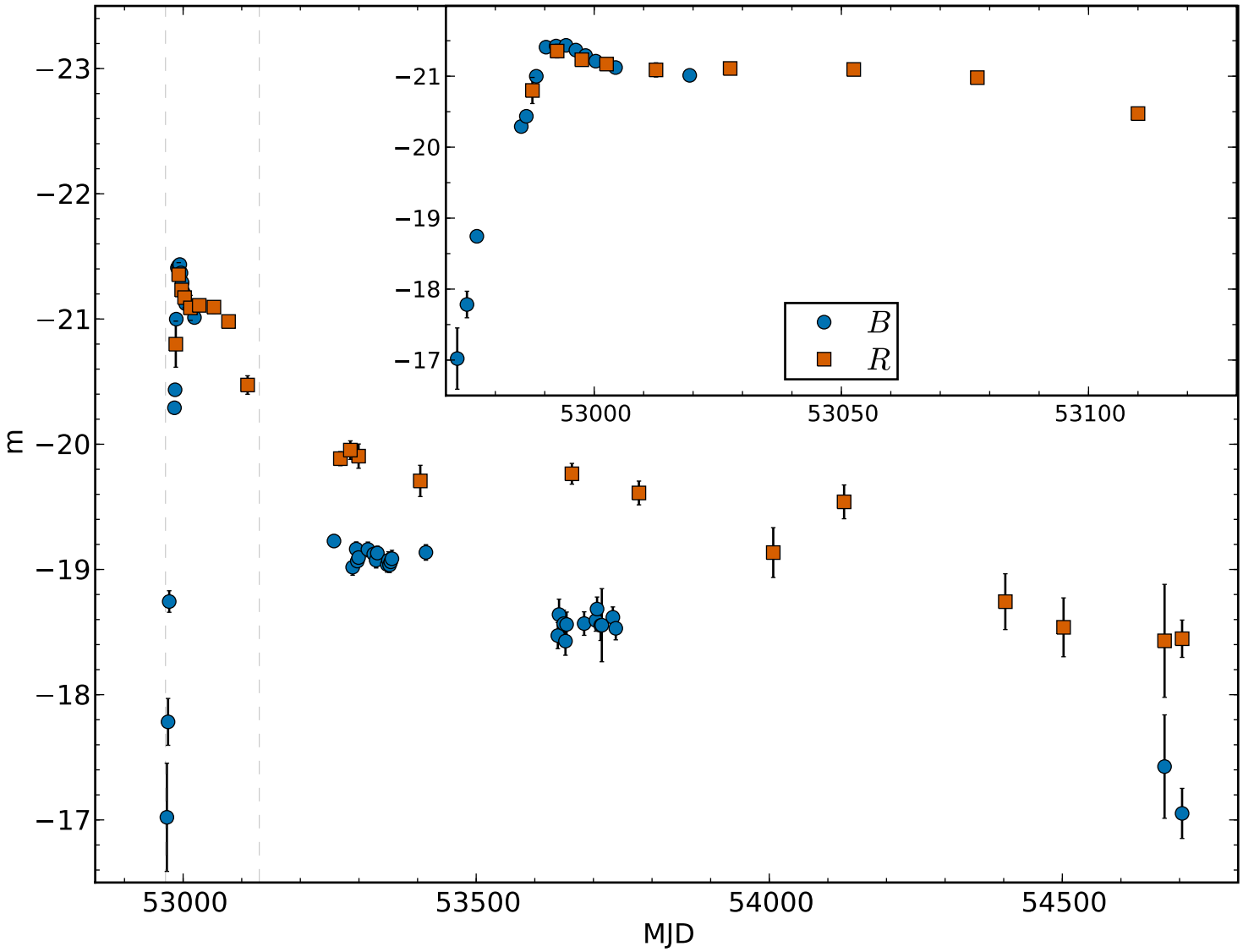
m
MJD
B
R
−23
−22
−21
−20
−19
−18
−17
53000
53500
54000
54500
53050
53100